NEUROSCIENCE

Facial expressions of emotion states and their neuronal correlates in mice

Nejc Dolensek[1,2], Daniel A. Gehrlach[1,3], Alexandra S. Klein[1,3], Nadine Gogolla[1]*

Understanding the neurobiological underpinnings of emotion relies on objective readouts of the emotional state of an individual, which remains a major challenge especially in animal models. We found that mice exhibit stereotyped facial expressions in response to emotionally salient events, as well as upon targeted manipulations in emotion-relevant neuronal circuits. Facial expressions were classified into distinct categories using machine learning and reflected the changing intrinsic value of the same sensory stimulus encountered under different homeostatic or affective conditions. Facial expressions revealed emotion features such as intensity, valence, and persistence. Two-photon imaging uncovered insular cortical neuron activity that correlated with specific facial expressions and may encode distinct emotions. Facial expressions thus provide a means to infer emotion states and their neuronal correlates in mice.

Emotions are patterns of behavioral, hormonal, and autonomic responses aimed at promoting survival. Emotions result from brain states that reflect the dynamic integration of external cues, bodily signals, and cognitive processes (*1*–*5*). Although emotions have been subject to intensive research efforts in neuroscience, psychology, and philosophy (*1*, *4*, *6*, *7*), we still lack a mechanistic understanding of how emotions arise in neuronal circuits (*3*, *4*, *8*, *9*). The functional dissection and causal interrogation of the neuronal circuit underpinnings of emotion rely on research in animal models. However, whether animals experience emotions similar to those of humans and how to best define or investigate emotions are still matters of controversy (*3*, *5*, *8*–*10*). Although most researchers would agree that externally observable behaviors indicate that forms of evolutionarily conserved "emotion states" exist across species (*1*, *3*, *5*), investigating emotions using modern neuroscientific tools has been hindered by a lack of rapid and precise readouts of emotion states in model organisms, such as mice (*3*).

In humans and monkeys, facial expressions have been proposed to provide universal indicators of emotions (*11*, *12*). Rodents may also use their orofacial musculature to signal longer-lasting internal states (*13*–*15*). We asked whether mice reacted to emotionally salient stimuli with stereotyped facial expressions and whether these reflect core emotion properties, such as intensity, valence, flexibility, and persistence (*3*, *4*). We then investigated neuronal correlates of inferred emotion states in the insular cortex, an area of the brain that in humans has been implicated in subjective affective experiences (*16*, *17*).

To study facial expressions, we exposed mice to a diverse set of sensory stimuli that can be assumed to trigger changes in emotion state. In addition to these triggers, we also monitored spontaneous behavioral expressions of emotion states, such as the exhibition of established fear behaviors. These "emotion events" of different types therefore included painful tail shocks, sweet sucrose, bitter quinine, and lithium chloride injections, which induce visceral malaise (*14*, *18*), as well as freezing and escape behaviors (see methods). We video monitored the faces of head-fixed mice (Fig. 1A and fig. S1, A and B). Mice reacted to each emotion event with a noticeable facial movement visible to naïve human observers (Fig. 1B, fig. S2A, and movie S1). However, the valence or type of the underlying emotion event was not intuitively recognizable (fig. S2, B and C) and required extensive experience (Fig. 1B).

To achieve objective and temporally precise classification of facial expressions we used machine vision. We chose "histogram of oriented gradients" (HOG) (*19*) descriptors to represent the statistics of local image features in a standardized way and provide one numerical vector for each video frame (see materials and methods for advantages of the HOG method). This allowed us to compare facial expressions of mice reacting to emotion events quantitatively through comparison of their corresponding HOG descriptors.

We first assessed the facial expressions resulting from each type of emotion event separately by comparing all video frames collected in the vicinity (before and after) of three repetitions of the same event in individual mice. Pairwise correlations of all frames in these clips rendered two discrete clusters of highly similar facial expressions: One cluster belonged to the pre-event epochs, and the second cluster belonged to the epochs during or immediately after the event (Fig. 1, C and D). No distinct clusters and thus no consistent change in facial expressions were detected when frames were selected in the same temporal sequence but from mice recorded during a baseline period (see "neutral" condition, Fig. 1D, top).

Next, we examined whether facial expressions were specific to the underlying emotion and visualized frames from all of the emotion events using t-distributed stochastic neighbor embedding (t-SNE). We observed a clean separation into discrete frame clusters for each event type within individual mice, suggesting emotion-specific facial expressions (Fig. 1E and fig. S3).

To test whether the underlying emotion event in any given mouse could be predicted solely from its facial expressions, we trained a random forest classifier (see materials and methods). The decoder could predict each underlying emotion event across different mice reaching accuracies >90%. Performance dropped on average below 15% if the decoder was trained on temporally shuffled data (Fig. 1F, fig. S4, and table S1).

These results raised the question of whether the observed expressions may reflect separate basic emotion states, similar to emotion categories in humans (*7*, *10*). We collected the most characteristic video frames following each type of emotion event separately and averaged the corresponding HOG vectors into a single descriptor (Fig. 2A and materials and methods), which we termed "emotion prototype." We constructed prototypical HOG descriptors assuming the following event ≈ *emotion state* contingencies: quinine ≈ *disgust*, sucrose ≈ *pleasure*, tail shock ≈ *pain*, lithium chloride ≈ *malaise*, escape ≈ *active fear*, and freezing ≈ *passive fear*.

We first tested the sufficiency of the prototypes to capture the characteristics of the distinct facial expressions across individuals (Fig. 2, B and C, fig. S5, and table S1). We measured the similarity of facial expressions to the emotion prototypes and, indeed, each single prototype was specific to only one emotion state, except for the active fear prototype, which resembled facial expressions evoked by bitter, pain, and escape and may thus capture features of diverse emotion states (Fig. 2C). Comparing each frame of any video sequence across time to an emotion prototype captured the dynamics of facial expressions at high resolution (fig. S6 and movie S2).

Although our results so far suggested that facial expressions may relate to internal emotion states, an alternative explanation could be that facial expressions are stereotyped, reflex-like reactions. We therefore aimed to test whether facial expressions reflected fundamental features of emotions (*3*, *4*), such as intensity, valence, generalization, flexibility, and persistence (Fig. 2, D to G).

Scalability refers to the observation that emotions vary by intensity (*3*, *5*). We thus

[1]Circuits for Emotion Research Group, Max Planck Institute of Neurobiology, Am Klopferspitz 18, 82152 Martinsried, Germany. [2]Graduate School of Systemic Neurosciences, Ludwig-Maximilians University Munich, Germany. [3]International Max-Planck Research School for Molecular Life Sciences, Munich, Germany.
*Corresponding author. Email: ngogolla@neuro.mpg.de

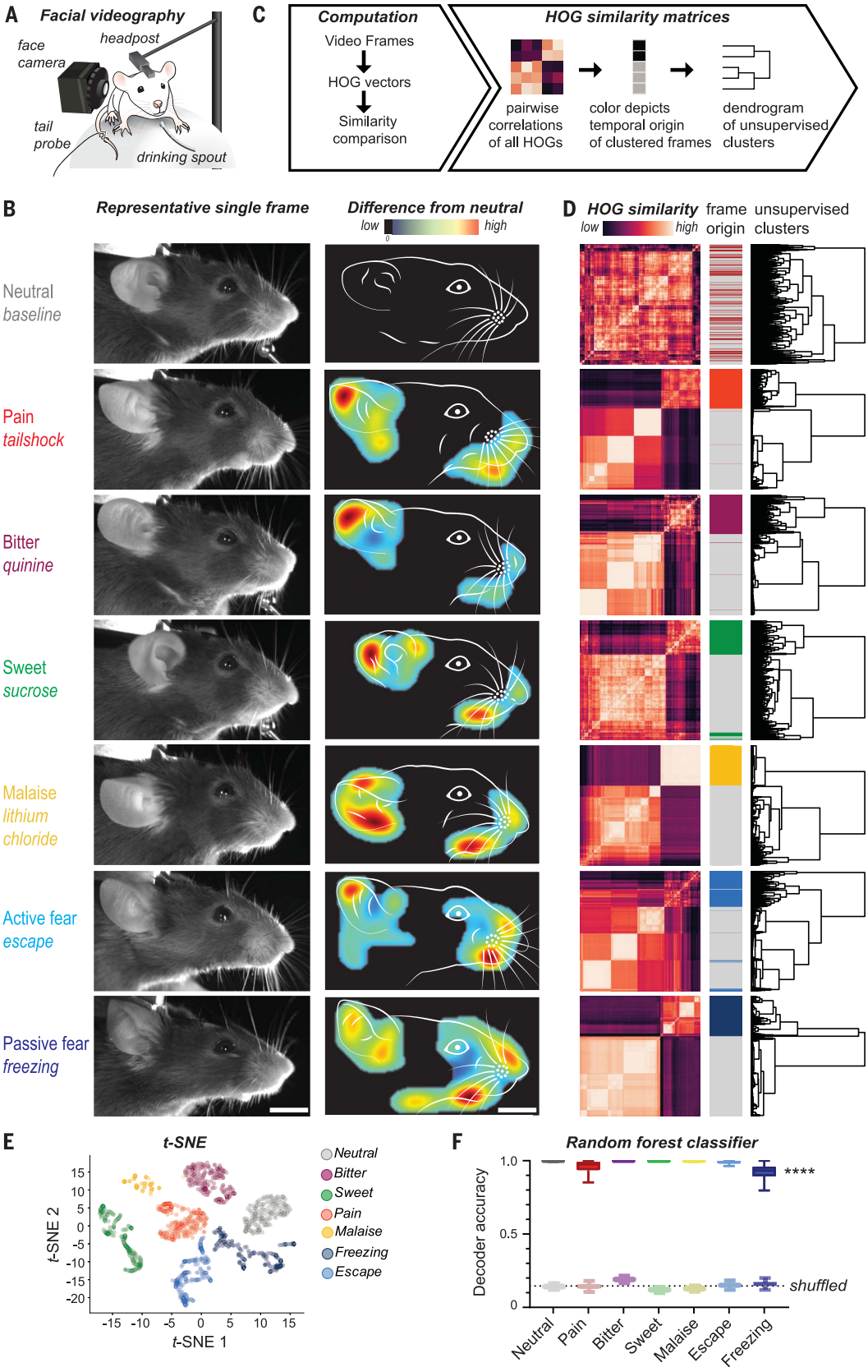

Fig. 1. Emotion-driven facial expressions in mice. (**A**) Facial videography setup. (**B**) (Left) Single representative video frames from individual mice captured during baseline (top) or upon different emotion events to illustrate characteristic changes. Images derived from N = 2 mice. Similar facial expressions were observed in all animals reported here. (Right) Line drawing of faces from the same frames. Heat-map overlays denote areas of largest difference compared to the neutral expression. Scale bar: 6 mm. (**C**) Computational strategy to compare facial expressions. (**D**) Similarity matrices containing pairwise similarity coefficients for all frames obtained in the vicinity of three events for each condition within one animal. To the right, post hoc temporal assignments for each frame are shown in color during the event and in gray before each event. Dendrograms represent hierarchical clustering. (**E**) t-SNE visualization of frames obtained from all emotion events in an individual mouse. (**F**) A random forest classifier reliably predicts and distinguishes between all event-related facial expressions. The classifier reaches high decoding accuracies (neutral, bitter, and sweet: 99 ± 1%; pain: 96 ± 5%; freezing: 92 ± 7%; malaise and escape: 99 ± 2%). Decoder performance dropped if the decoder was trained on temporally shuffled data (neutral: 14 ± 1%; bitter: 19 ± 1%; sweet 12 ± 1%; malaise: 13 ± 1%; pain: 14 ± 2%; freezing: 16 ± 2%; escape: 15 ± 1%). Mann-Whitney test revealed a significant (****P < 0.0001) difference in classifier's prediction performance between the real and shuffled data for each single facial expression.

varied the stimulus strength and quantified the similarity of the resulting facial expressions to our prototypes. The similarity to prototypical descriptors increased significantly and in a graded manner when the strength of tail shocks, or the concentration of sucrose or quinine solutions, increased (Fig. 2D and table S1), although the sequence of stimulation did not influence the facial expression intensity at the chosen intertrial intervals (fig. S7, A and B).

Another property of emotions is their valence—namely, they are experienced as good or bad in humans and trigger approach or retreat in animals (*3*, *5*, *14*, *18*). Salt is appetitive for rodents at low concentrations but aversive at high

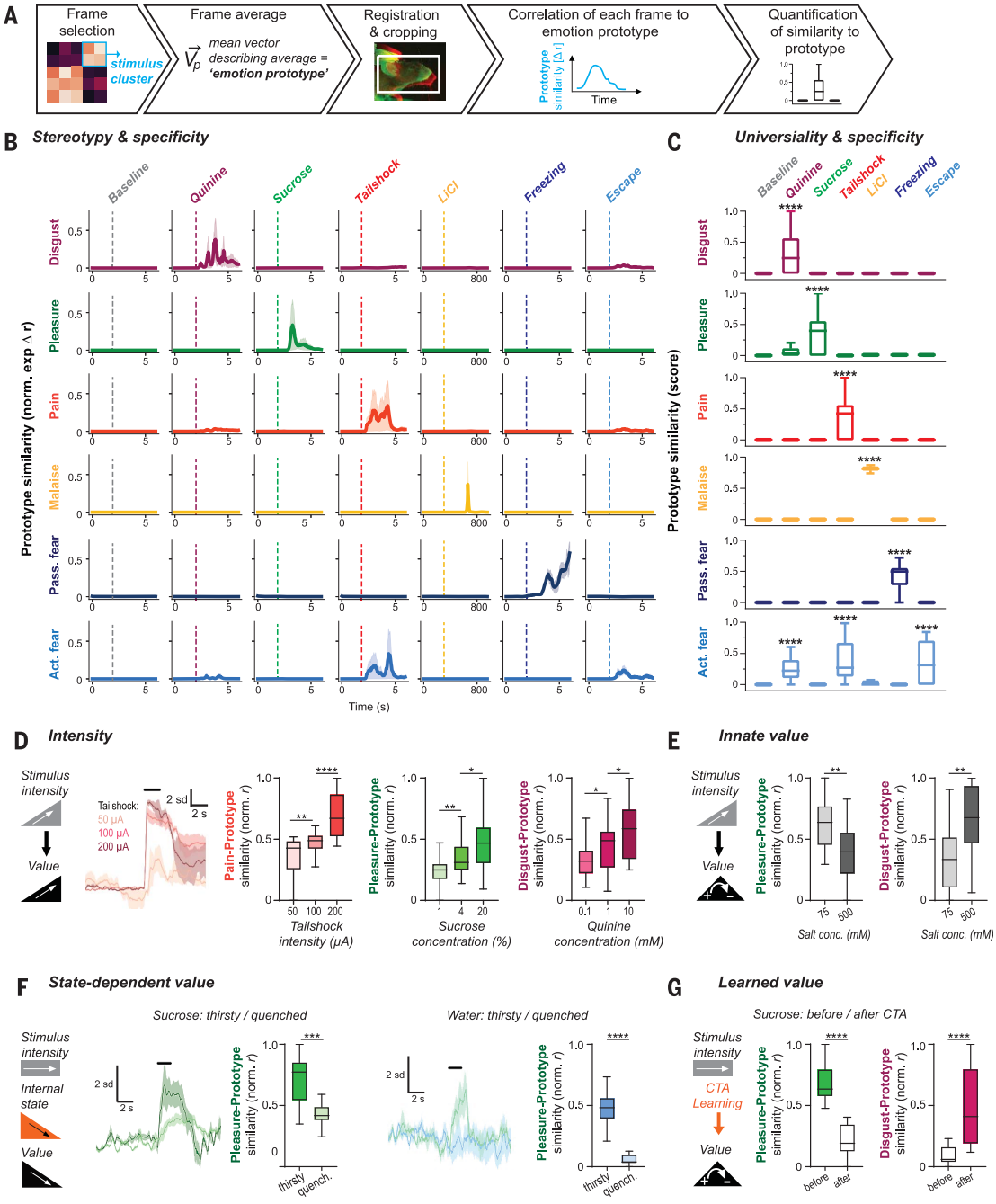

Fig. 2. Facial expressions reflect core features of emotion states. (**A**) Schematic of emotion prototype creation. (**B**) Similarities of facial expressions for each event type (three occurrences each) in one exemplary mouse to each emotion prototype. (**C**) Prototypes are valid and specific universally across mice. To calculate a similarity score, data from $N = 9$ mice and $n = 27$ trials per stimulus were averaged, then min-max normalized; the highest similarity value was set to 1, and the maximal baseline value and negative values were set to 0. Facial expressions were highly experience specific [ordinary one-way analysis of variance, $^{****}P < 0.0001$, Dunnett's post hoc comparisons revealed significant differences ($^{****}P < 0.0001$) to the neutral condition only for the event matching the prototype, except for escape which carried components of pain and disgust.] (**D**) Sensory stimuli of increasing strength elicit more intense facial expressions. (Left) Example traces of face similarities to the pain prototype in one example mouse experiencing increasingly strong tail shocks. To the right, box-and-whisker plots quantifying the facial expression similarity to the pain prototype upon increasing tail shock intensities ($N = 9$ mice, $n = 27$ trials per intensity); the pleasure similarity upon drinking solutions of increasing sucrose content ($N = 9$ mice, $n = 27$ trials per concentration); and disgust similarity upon drinking solutions of increasing quinine content ($N = 10$ mice, $n = 30$ trials per concentration). (**E**) Drinking solutions of low salt content (75 mM) evoke pleasure-like facial expression (left) but little disgust-like facial expressions (right). The inverse pattern was observed upon drinking solutions with high salt content (500 mM). $N = 5$ mice, $n = 15$ trials per concentration. (**F**) Facial expressions reveal the changing affect upon experiencing sucrose or water in either thirsty or quenched states. $N = 5$ mice, $n = 15$ trials per state. (**G**) Facial expressions reveal associative aversion learning. Mice expressed highly pleasurable and low disgust facial expressions when drinking sucrose solutions before CTA. After CTA, mice exhibited disgusted facial expressions and low pleasure when drinking sucrose. $N = 5$ mice, $n = 15$ trials per timepoint. In all panels: $^{*}P \leq 0.05$, $^{**}P \leq 0.01$, $^{***}P \leq 0.001$, $^{****}P < 0.0001$, two-tailed Mann-Whitney tests. Box-and-whisker plots in the style of Tukey containing trial averages. Line graphs are z-scored face similarities normalized to the 2 s preceding the stimulus, averaged across three trials in a single animal. Shaded areas are SEM.

concentrations. Facial expressions reflected the innate valence of salt at different concentrations, because salt at low concentration elicited facial expressions of high similarity to our prototypical "pleasure" facial expression and weak similarity to our "disgust" prototype, whereas the opposite was observed for high salt concentrations (Fig. 2E and table S1). Facial expressions are thus decoupled from the underlying stimulus and generalize between different sensory experiences. Both sucrose and low-concentration salt solution elicited pleasure-like expressions, whereas quinine and high-concentration salt solution both evoked disgust.

Emotions reflect an integrated account of external and internal information (*3*, *9*) and are thus flexible. We next varied the internal state of the animal but kept the stimulus constant. When mice drank an identically concentrated sucrose solution or water in either thirsty or quenched states, both liquids elicited significantly stronger pleasure-like facial expressions when mice were thirsty than when they were quenched (Fig. 2F and table S1).

Emotions are thought to arise from predictions about how internal or external events may affect the well-being of the individual (or the well-being of closely related conspecifics) (*1*, *9*, *10*). These predictions can depend on the innate or learnt value of stimuli. We already saw how the innate value of salt depended on its concentration. Would learning affect facial expressions in a similar way? We exposed mice to sucrose solution and then injected them with malaise-inducing lithium chloride to induce conditioned taste aversion (CTA). Sucrose

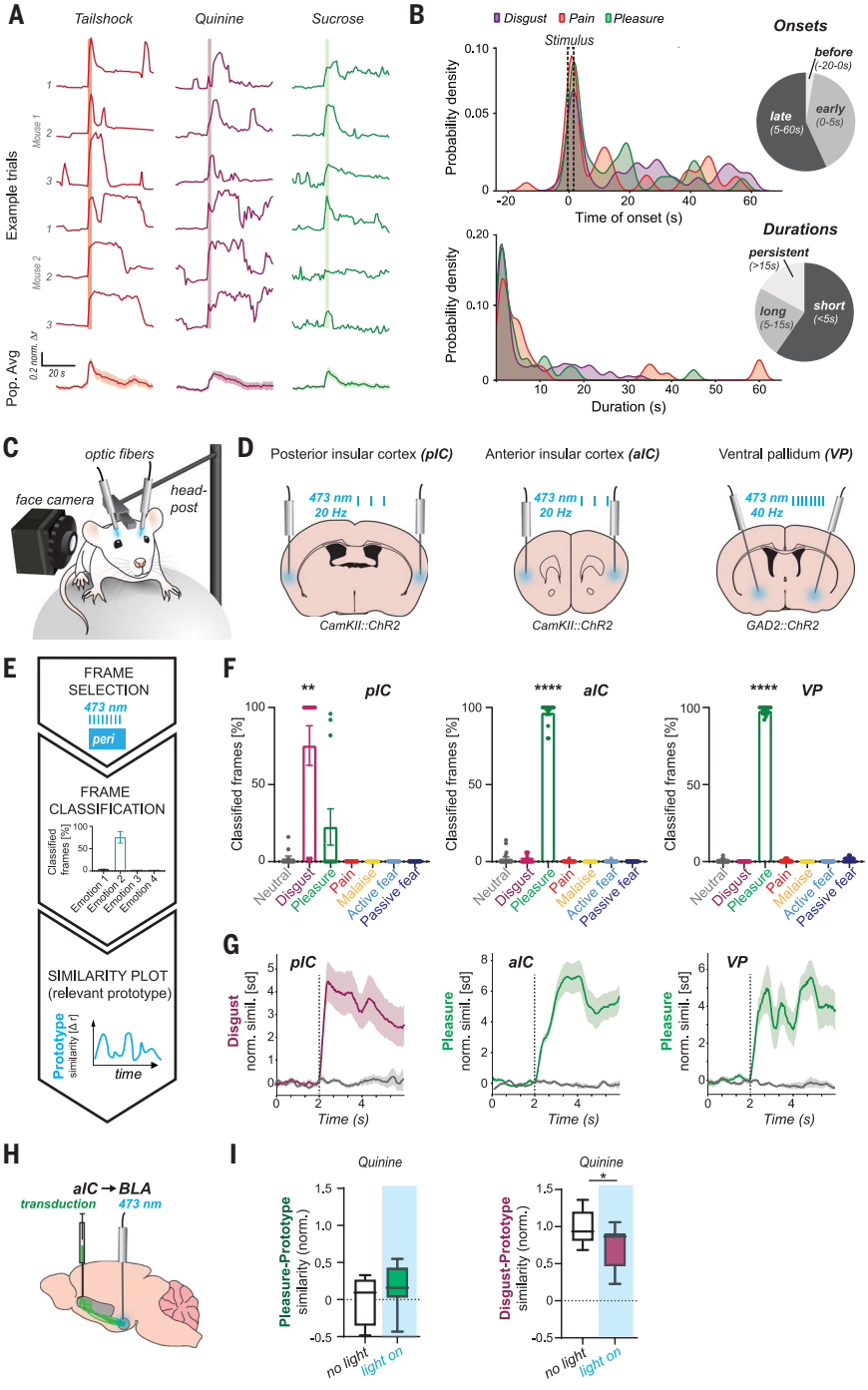

Fig. 3. Facial expressions are variable and associated with internal brain states. (**A**) Similarity traces (1-s binned) for each relevant emotion prototype (tail shock, pain prototype; quinine, disgust prototype; sucrose, pleasure prototype). (Top) Individual event-triggered facial expression traces exhibit great variability within the same individual and across mice. (Bottom) Population average (pain and sucrose N = 9 animals, n = 27 trials; quinine N = 10 animals, n = 30 trials). Shaded area: 95% confidence interval. (**B**) Quantification of facial expression onsets (top) and durations (bottom). Probability density is based on kernel density estimates. (**C**) Experimental approach for combined facial videography and optogenetic circuit manipulations to elicit changes in internal brain states. (**D**) Optogenetic stimulation sites in the posterior insular cortex (pIC), anterior insular cortex (aIC), and ventral pallidum (VP). (**E**) Experimental strategy to determine the nature of the optogenetically evoked facial expressions and their description. (**F**) Individual frames for each optogenetic stimulation epoch were individually classified. For each emotion, the average fraction of classified frames was then plotted per trial (pIC, n = 12 trials, N = 4 mice; aIC and VP, n = 18 trials, N = 6 mice). One sample Wilcoxon test revealed significantly higher detection values than random (14.3%) only for one emotion for each optogenetic condition: disgust for pIC and pleasure for aIC and VP (****P < 0.0001). (**G**) Plot of the normalized similarity (Pearson's r) for all pre- and peri-event frames against the prototype as suggested by the classifier (dashed line indicates stimulus onset). Lines are mean z-scored face similarities across all trials (as above) with shaded areas representing the SEM. Colored lines from animals expressing ChR2 (channelrhodopsin-2), gray lines from control animals expressing eYFP (enhanced yellow fluorescent protein). (**H**) Optogenetic strategy to activate the aIC→BLA pathway. (**I**) Animals were exposed to quinine for 2 s under control ("no light") and optogenetic activation ("light on") of the aIC→BLA pathway. n = 9 trials from N = 3 mice. Similarities were normalized so that during no-light conditions, the mean value for pleasure = 0 and mean value for disgust = 1 in order to reveal the changes from the previously established baseline values.

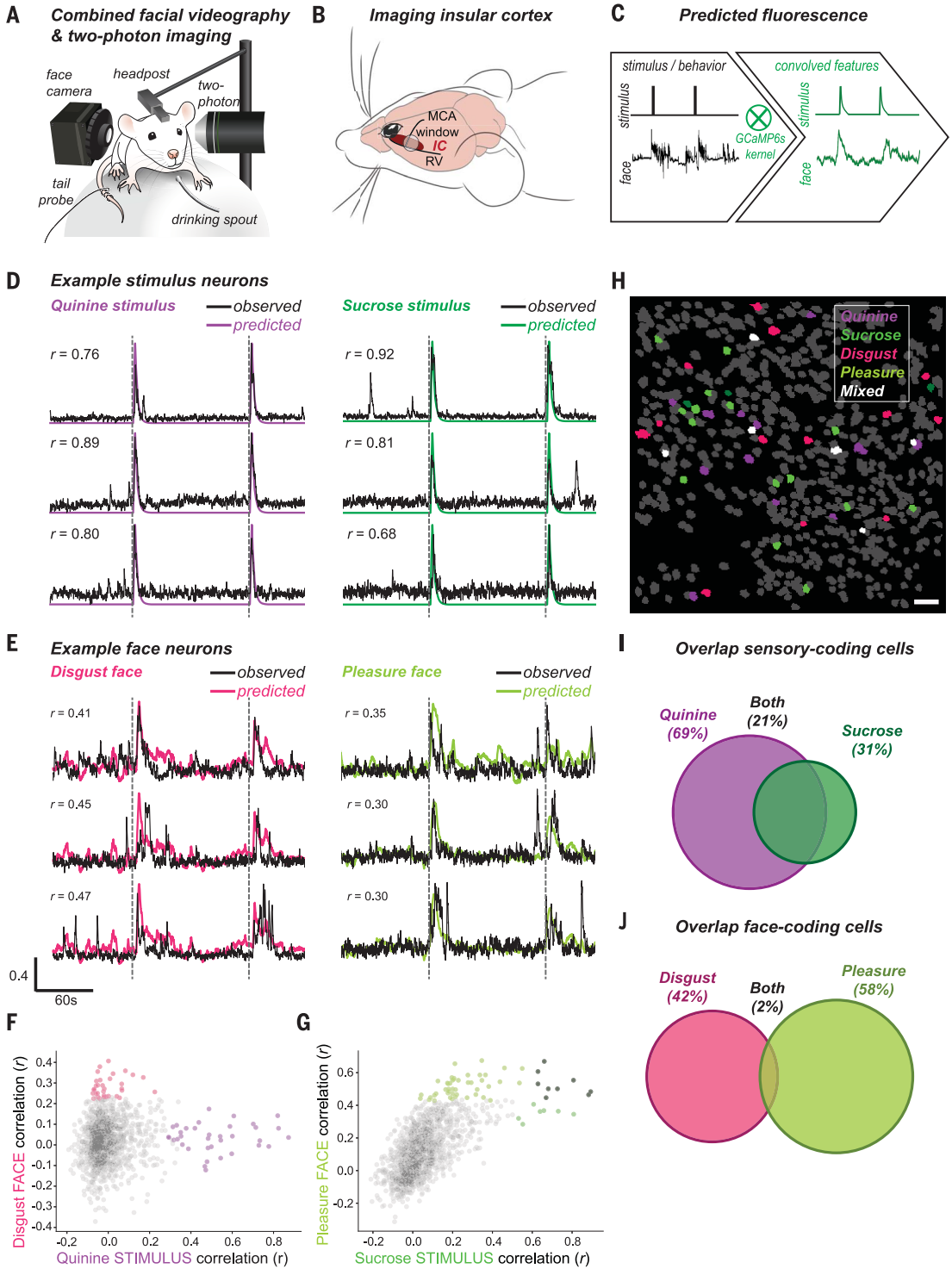

Fig. 4. Neuronal correlates of emotion state in the posterior insular cortex. (**A**) Illustration of combined facial videography with awake two-photon calcium imaging. (**B**) Schematic of the chronic window implant above the posterior insular cortex (IC, red) with respect to major blood vessels: medial cerebral artery (MCA) and rhinal vein (RV). (**C**) Schematic of neuronal activity prediction through stimulus and face convolution with GCaMP6s kernel. (**D** and **E**) Representative normalized fluorescence traces (black) overlaid with predicted stimulus or facial expression traces (colored). R values are Pearson's *r* for the correlation between normalized fluorescence and the overlaid convolved trace. (**F**) Scatter plot containing 1198 neurons from two animals experiencing quinine, plotted on the basis of their correlation to the convolved stimulus trace (quinine) and convolved face similarity trace (disgust prototype) for three stimulus presentations. A subset of neurons correlated strongly to the disgust similarity trace is labeled pink. A subset of neurons correlated strongly to the quinine stimulus trace is colored purple (for thresholds, see materials and methods). (**G**) Same as (F), but with sucrose stimulus. Neurons most strongly correlated to the pleasurable facial expression are labeled light green, neurons most strongly correlated to sucrose stimulus are in dark green, and the subset of neurons highly correlated to both are colored black (for thresholds, see materials and methods). (**H**) An example field of view from one animal with labeled regions of interest (ROIs) (gray circular shapes). Neurons, as identified and labeled in (F) and (G), are overlaid with the appropriate color. White ROIs indicate neurons with mixed coding properties (mostly multisensory neurons). (**I** and **J**) Venn diagrams representing the overlap in coding properties between sensory-coding cells (I) and face-coding cells (J). Scale bar: 100 μm.

before CTA learning elicited pleasure but not disgust. After CTA learning, mice displayed disgusted facial expressions in response to sucrose and thus their expressions reflected the learnt change in subjective value of sucrose (Fig. 2G and table S1).

Emotions are thought to reflect complex internal brain states. Because we cannot control all emotion-relevant information streams, one would hypothesize that even under identical stimulus conditions, the triggered emotion state should vary. We therefore analyzed the variability of stimulus-triggered facial expressions. Within the same mouse but also across different mice, repeating the same stimulus elicited facial expressions that varied in intensity, onset, and duration (Fig. 3, A and B). Facial expressions could wane and

spontaneously reappear, possibly reflecting dynamic fluctuations in the underlying emotion state (Fig. 3A). Although the great majority of stimulus presentations resulted in immediate facial expressions (~90% of stimuli evoked facial expressions within 5s of stimulus onset), a considerable number of overall facial expressions occurred late after the stimulus (>5 s after stimulus start). Similarly, the duration of facial expressions was highly variable. Most facial expressions triggered by 2-s-long sensory stimuli lasted for less than 5 s (~60%); however, a substantial fraction of facial expressions lasted for relatively long periods (5- to 15-s duration, ~23%), or even persisted for more than 15 s (~17%) (Fig. 3B).

Direct brain stimulations can evoke specific emotions (*20*, *21*). We used optogenetics to test whether manipulating activity in emotion-relevant neuronal circuits could drive facial expressions (Fig. 3, C and D). We activated subregions and specific projections of the insular cortex (IC) that have been shown in humans and animals to evoke emotional sensations and behaviors (*20*, *22*–*25*). Furthermore, we manipulated the γ-aminobutyric acid–releasing neurons in the ventral pallidum (VP) that process rewarding properties of pleasant stimuli (*26*) (Fig. 3D). Each region-specific optogenetic manipulation evoked strong facial expressions (fig. S8 and movie S3). To analyze whether the evoked facial expressions would fall into our previously created emotion-state categories, we used the same random forest classifier as in Fig. 1F and categorized all frames during the optogenetic stimulations (Fig. 3, E and F). For each of these three manipulations, the classifier identified one specific emotion to be displayed—namely, pleasure—for the anterior IC and VP, but disgust for the posterior IC stimulations (Fig. 3F and table S1). When we compared the optogenetically evoked facial expressions to our emotion prototypes, we found a similar temporal build-up and persistence of the facial expressions to those triggered externally (Fig. 3G and movie S3). Projections from the insular cortex to the amygdala can influence the emotional value of tastants (*25*). Indeed, in agreement with this earlier report, the activation of the anterior IC→basolateral amygdala (aIC→BLA) pathway during the exposure to quinine attenuated the expression of disgust (Fig. 3, H and I).

Our data so far suggest that facial expressions are sensitive reflections of internal emotion states, which correspond to brain states. Therefore, we assumed that facial expressions should have neuronal correlates in emotion-relevant brain regions. The insular cortex is a critical brain region for emotional experience and behavior (*16*, *17*, *20*–*24*). We combined facial videography with two-photon calcium imaging in the posterior IC (pIC) to search for neuronal correlates of facial expressions (Fig. 4, A and B, and fig. S9). We identified single neurons that reliably encoded sensory stimuli in the pIC (Fig. 4, C to G), consistent with previous studies (*22*, *27*). We also identified neurons that exhibited strong correlations to the facial expression dynamics and only low correlations with the stimuli (Fig. 4, D to G). Indeed, these "face" neurons captured the characteristic persistence and spontaneity of the facial expression. Although a substantial fraction of stimulus neurons was multisensory, face-responsive neurons were highly segregated and exhibited almost no overlap.

In this study, we have identified facial expressions as reliable indicators of emotion states and their neuronal correlates in mice. But why do mice exhibit facial expressions? Charles Darwin suggested that facial expressions reveal affective processes across species, implying an evolutionarily conserved function of these behaviors (*1*). Though often discussed in the context of social communication, facial expressions may have evolved first as parts of emotional action programs, preparing for motor behaviors and adapting sensory acquisition to changes in the internal or external milieu (*2*, *28*, *29*). Indeed, head-fixed mice, which do not socially interact, consistently respond to emotionally salient events with stereotyped facial expressions. Although the value of facial expressions for uncovering emotional processes in humans remains controversial (*30*), this may be partially due to the volitional control that humans exert over emotions and their expression. It would therefore be interesting to examine how facial expressions are modified by the presence of conspecifics in mice.

Direct observation of facial expressions is possible in quasi–real time (fig. S10) and allows for the mechanistic investigation of the neural underpinnings of emotions in mice. Correlation of emotional facial expressions with neuronal activity recordings and closed-loop manipulations are promising approaches to search for and test the causal role of the neuronal substrates of basic emotional building blocks, such as intensity, valence, and persistence.

Our data suggest that facial expressions can be classified into different basic categories. An important question for future studies may be to what degree emotion states are dimensional or categorical states at the level of not only behavioral expressions but also the underlying brain circuitries. The relatively simple implementation of HOG feature descriptors may become a useful addition to studying emotional facial or postural expressions in other laboratory animals, such as rats, shrews, lemurs, and monkeys. It may also help in identifying unknown, species-specific emotion states and assist in moving toward a more universal and evolutionarily based definition and understanding of emotions and their neural underpinnings across species.

REFERENCES AND NOTES

1. C. Darwin, *The Expression of the Emotions in Man and Animals* (London, Murray, 1872).
2. A. Damasio, G. B. Carvalho, *Nat. Rev. Neurosci.* **14**, 143–152 (2013).
3. D. J. Anderson, R. Adolphs, *Cell* **157**, 187–200 (2014).
4. Ralph Adolphs & David J. Anderson, *The Neuroscience of Emotion: A New Synthesis* (Princeton Univ. Press, 2018).
5. R. Adolphs, *Soc. Cogn. Affect. Neurosci.* **12**, 24–31 (2017).
6. J. A. Russell, *J. Pers. Soc. Psychol.* **39**, 1161–1178 (1980).
7. P. Ekman, *Cogn. Emotion* **6**, 169–200 (1992).
8. J. LeDoux, *Neuron* **73**, 653–676 (2012).
9. L. F. Barrett, A. B. Satpute, *Neurosci. Lett.* **693**, 9–18 (2019).
10. J. Panksepp, *Neurosci. Biobehav. Rev.* **35**, 1791–1804 (2011).
11. P. Ekman, *Philos. Trans. R. Soc. Lond. B Biol. Sci.* **335**, 63–69 (1992).
12. L. A. Parr, B. M. Waller, J. Fugate, *Curr. Opin. Neurobiol.* **15**, 716–720 (2005).
13. D. J. Langford *et al.*, *Nat. Methods* **7**, 447–449 (2010).
14. A. Faure, J. M. Richard, K. C. Berridge, *PLOS ONE* **5**, e11223 (2010).
15. K. Finlayson, J. F. Lampe, S. Hintze, H. Würbel, L. Melotti, *PLOS ONE* **11**, e0166446 (2016).
16. J. Chikazoe, D. H. Lee, N. Kriegeskorte, A. K. Anderson, *Nat. Neurosci.* **17**, 1114–1122 (2014).
17. N. Gogolla, *Curr. Biol.* **27**, R580–R586 (2017).
18. P. Tovote, J. P. Fadok, A. Lüthi, *Nat. Rev. Neurosci.* **16**, 317–331 (2015).
19. N. Dalal, B. Triggs, in *2005 IEEE Computer Society Conference on Computer Vision and Pattern Recognition, CVPR 2005* (2005), vol. 1, pp. 886–893.
20. F. Caruana, A. Jezzini, B. Sbriscia-Fioretti, G. Rizzolatti, V. Gallese, *Curr. Biol.* **21**, 195–199 (2011).
21. C. Fausto, *Emot. Rev.* **11**, 27–38 (2019).
22. D. A. Gehrlach *et al.*, *Nat. Neurosci.* **22**, 1424–1437 (2019).
23. J. Yih, D. E. Beam, K. C. R. Fox, J. Parvizi, *Soc. Cogn. Affect. Neurosci.* **14**, 339–351 (2019).
24. Y. Peng *et al.*, *Nature* **527**, 512–515 (2015).
25. L. Wang *et al.*, *Nature* **558**, 127–131 (2018).
26. L. Faget *et al.*, *Nat. Commun.* **9**, 849 (2018).
27. X. Chen, M. Gabitto, Y. Peng, N. J. P. Ryba, C. S. Zuker, *Science* **333**, 1262–1266 (2011).
28. C. Montag, J. Panksepp, *Motiv. Emot.* **40**, 760–766 (2016).
29. J. M. Susskind *et al.*, *Nat. Neurosci.* **11**, 843–850 (2008).
30. L. F. Barrett, R. Adolphs, S. Marsella, A. M. Martinez, S. D. Pollak, *Psychol. Sci. Public Interest* **20**, 1–68 (2019).
31. N. Dolensek, N. Gogolla, GogollaLab/MouseFacialExpressionAnalysis, Version 1.0, Zenodo (2020).

ACKNOWLEDGMENTS

We thank members of the Gogolla laboratory, K. Branson, P. Dayan, W. Denk, M. Hübener, E. Mace, D. Mearns, R. Portugues, and A. Sirota for discussions; J. Kuhl (somedonkey.com) for illustrations; and T. Black, F. Lyonnaz, A. Podgornik, and C. Weiand for technical assistance. **Funding:** Supported by the Max-Planck Society, the European Research Council (ERC) under the European Union's Horizon 2020 research and innovation program (ERC-2017-STG, grant agreement no. 758448 to N.G.), the Deutsche Forschungsgemeinschaft (SPP1665), the German Israeli Foundation (Grant I-1301-418.13/2015), and the ANR-DFG project "SAFENET" (ANR-17-CE37-0021). **Author contributions:** N.G. and N.D. conceived the project and designed the experiments. N.D. performed all experiments and developed and performed all facial expression analysis. D.A.G. and A.S.K. helped with the optogenetic experiments. N.G. wrote the manuscript with assistance from N.D. **Competing interests:** The authors declare no competing financial interests. **Data and materials availability:** All data are available in the manuscript or the supplementary materials. The facial expression analysis code is available on Github (https://github.com/GogollaLab) and at Zenodo (*31*). Viruses were packaged at the University of North Carolina (UNC) Vector Core and made available under a material transfer agreement.

SUPPLEMENTARY MATERIALS

science.sciencemag.org/content/368/6486/89/suppl/DC1
Materials and Methods
Figs. S1 to S10
Table S1
Movies S1 to S3
References (*32*–*41*)

View/request a protocol for this paper from *Bio-protocol*.

22 October 2019; accepted 11 February 2020
10.1126/science.aaz9468

science.sciencemag.org/content/368/6486/89/suppl/DC1

Supplementary Materials for

Facial expressions of emotion states and their neuronal correlates in mice

Nejc Dolensek, Daniel A. Gehrlach, Alexandra S. Klein, Nadine Gogolla*

*Corresponding author: ngogolla@neuro.mpg.de

Published 3 April 2020, *Science* **368**, 89 (2020)
DOI: 10.1126/science.aaz9468

This PDF file includes:

Other Supplementary Materials for this manuscript include the following:
(available at science.sciencemag.org/content/368/6486/89/suppl/DC1)

Movies S1 to S3

Materials and Methods

Animals

All procedures were approved by the Government of Upper Bavaria. Male and female mice at 2-6 months of age were housed in groups of 2 or 3 animals and kept on a 12 h inversed light cycle (11:00 a.m., lights off). Mice were provided with ad libitum access to standard chow and water except for drinking and CTA experiments, when mice were water deprived for periods of time specified in the following sections. All behavioral experiments were conducted with C57BL/6NRj mice, imaging experiments were performed on transgenic tetO-GCaMP6s [JAX 024742] x CaMKII-tTA [JAX 007004] mice and optogenetic experiments were performed on C57BL/6NRj and GAD2-Cre mice [JAX 010802].

Viral constructs

For in-vivo optogenetic experiments, the following constructs were obtained from the UNC Vector Core (Gene Therapy Center, University of North Carolina at Chapel Hill, USA): AAV2/5-CaMKIIa-hChR2(H134R)-eYFP ($6.2x10^{12}$ vg/ml), AAV2/5-CaMKIIa-eYFP ($4.3x10^{12}$ vg/ml), AAV2/5-EF1a-DIO-eYFP ($5.6x10^{12}$ vg/ml) and AAV2/5-EF1a-DIO-hChR2(H134R)-eYFP ($5.5x10^{12}$ vg/ml).

Surgical procedures

We injected metamizol (200 mg/kg, s.c.) for peri-operative analgesia and carprofen (s.c., 5 mg/kg, once daily for 3 days) for post-operative pain care.

Head-post implantation for facial videography

Mice were anaesthetized using midazolam / medetomidin / fentanyl mix (5mg/kg; 0.5 mg/kg; 0.05 mg/kg). Lidocaine was applied topically at the incision site. A head post was secured to the skull using C&B Super-Bond (Sun Medical).

Cranial window surgery for two-photon calcium imaging

Mice (tetO-GCaMP6s x CaMKII-tTA) were anaesthetized using midazolam / medetomidin / fentanyl mix (5 mg/kg; 0.5 mg/kg; 0.05 mg/kg) and injected with dexamethasone (s.c., 0.2 mg/kg). Lidocaine was applied topically at the incision site. A head post was secured to the skull using C&B Super-Bond (Sun Medical). Tissue including parts of the temporalis muscle was

removed and the skull was cleaned above the left insular cortex. A craniotomy was created using a 3 mm biopsy punch (Miltex) and positioned with the rhinal vein as the ventral limit and the medial cerebral artery slightly anterior to the center of the window, as seen through the skull. Since cortical surface is curved, the brain was protected from being flattened by applying a small amount of transparent polymer as previously described (*31*). A 3 mm cover slip was gently positioned on top of the polymer and secured using cyanoacrylate glue. The remaining exposed skull was covered with C&B Super-Bond.

In-vivo optogenetic experiments

Anesthesia was initiated with 5% isoflurane and maintained at 1-2.5% throughout surgery. Mice were secured in a stereotaxic frame (Stoelting), placed on a heating pad (37 °C) and eye ointment (Bepanthen, Bayer) was applied. We performed bilateral skull trepanations for all optogenetic experiments. For all viral injections, we used pulled glass-pipettes attached to a microliter syringe (5 µL Model 75 RN, Hamilton) using a glass needle compression fitting (#55750-01, Hamilton), mounted on a syringe pump controlled by a microcontroller (UMP3 + micro4, WPI). All injections were performed at a rate of 80 nl/min.

For aIC and pIC animals (C57BL/6NRj), we bilaterally injected 100 nl of virus (AAV2/5-CaMKIIa-hChR2(H134R)-eYFP or AAV-CamKIIa-eYFP for the control mice) into the aIC (distances from Bregma: AP: +1.7 mm, ML: ± 3.1 mm, DV: - 3.5 mm) or pIC (distances from Bregma: AP: -0.35 mm, ML: ± 4.05 mm, DV: - 4 mm). Custom-made optic fibers (200 µm core, 0.22 NA, 1.25 mm zirconia ferrule from Thorlabs) were implanted 0.5 mm above the injection site.

For ventral pallidum animals (GAD2-IRES-Cre) we bilaterally injected 80 nl of Cre-dependent virus (AAV2/5-EF1a-DIO-hChR2(H134R)-eYFP or AAV2/5-EF1α-DIO-eYFP for the control mice) into the ventral pallidum (distances from Bregma: AP: -0 mm, ML: ± 2.5 mm, DV: - 4.9 mm at 10° angle). Custom-made optic fibers (see above) were implanted 0.5 mm above the injection site.

For aIC→BLA projection specific manipulation, we bilaterally injected 50 nl of virus (AAV2/5-CaMKIIa-hChR2(H134R)-eYFP or AAV-CamKIIa-eYFP for the control mice) into the aIC (same coordinates as mentioned above) and bilaterally implanted optic fibers above the BLA (distances from Bregma: AP: -1.0 mm, ML: ± 3.2 mm, DV: - 3.8 mm). A head post was secured to the skull using C&B Super-Bond (Sun Medical). We sealed the space between the fiber and

the trepanation with bone wax to protect the underlying brain tissue from the cyanoacrylate glue (Ultra Gel, Pattex) that secured the optic fibers to the skull. Additionally, we added a layer of black colored dental cement to further secure the optic fibers and to reduce light emission from the skull.

Experimental timelines

All mice were handled by the experimenter for a period of at least 3 days prior to any surgical procedures. After a surgical procedure (described above), animals were allowed to rest for a period of 7-10 days. Following that, they were handled by the experimenter and habituated to head-fixation for a period of 5 days. For fixing to the head-holder on the setup, mice were briefly anesthetized with 5% isoflurane. After any head- fixation, the mice were always allowed at least 30 min to recover and habituate.

Orofacial videography

We acquired data at 30 Hz using a USB 3.0 monochrome camera (BFS-U3-13Y3M-C, Point Grey Research), positioned perpendicularly to the right side of the mouse's head. Illumination was provided by three 875 nm IR LED arrays (Kemo Electronic M120). See fig. S1 for schematic illustration of the camera and light arrangements. The camera was fitted with a NIR short-pass filter with a 900 nm cutoff (FES0900, Thorlabs) to filter out two-photon excitation light and a long-pass filter with 600 nm cutoff (FEL0600, Thorlabs) to filter out optogenetic stimulation light. Mice were weakly illuminated from behind by a 470 nm fiber coupled LED (M470F3, Thorlabs).

Stimulus deliveries and protocols

Timeline

All stimuli except where specified differently (see LiCl injection, safe/fearful context) were delivered to mice for 2 s after a baseline of 120 s in blocks of 3 repeated stimulations 120 s apart. The blocks of stimuli were separated by 500-1000 s when performed consecutively.

Stimulation sequence

Animals were exposed to sets of stimuli in blocks of 3 stimuli in a pseudo-randomized order. Strongly aversive stimuli, such as pain and malaise, were always presented as the last stimuli in an experiment.

Tastants

Tastants were presented to the animals' mouth through a round-ended reusable feeding needle (Fine Science Tools) for 2 s at a time, controlled using a solenoid pinch valve (P/N: 225PNC2-21, NResearch). Delivered tastants were: 1, 4, 20 % sucrose solution, 0.1, 1, 10 mM quinine solution, 75 and 500 mM NaCl solution (all Sigma Aldrich) and drinking water (from our animal facility). Trials were visually inspected to ensure the animals tasted the liquid presented.

Tailshocks

Weak electrical shocks (2 s; 50, 100 or 200 µA) were administered to the tail generated by a Precision animal shocker (Coulbourn Instruments). Two 0.5 mm silver-coated copper wire coils (Conrad), custom made for each mouse, were soldered to a lightweight isolated cable connected to the shocker and positioned approximately 1 cm apart at the center of the tail.

Lithium chloride induced malaise

While being head-fixed, animals were carefully injected i.p. with a lithium chloride solution (0.15 M LiCl in 0.9 % saline, 2 % body weight, e.g. 600 µl / 30 g mouse) and were recorded for a period of approximately 20 min.

Safe and fearful context

Safe context was defined as a context in which a mice has never experienced an aversive stimulus. Following a baseline recording in the safe context, mice repeatedly received unsignaled tailshocks across approximately 30 min. Mice were allowed to rest in their cage and were again placed on the behavioral setup 24 h later in what we then defined as fearful context.

Neutral / baseline condition

Neutral condition data was collected identically to all stimulus conditions, including the sampling from the same 2 s long stimulus time-points, however, no actual stimuli were presented. Furthermore, the mice were in a safe context to which they were well habituated and had no aversive experiences associated with it.

Thirst

Mice were acutely water deprived for 16-20 h and were presented with 20 % sucrose solution and water for 2 s, three times each, in a random order. Following that, they were repeatedly presented with drops of water across a period of 10 min and were allowed to drink to satiation. 5 min after that, they were again presented with drops of sucrose solution and water, identically to the start of the experiment. Trials were visually inspected to make sure that in all included trials animals tasted the liquids.

Conditioned taste aversion

Animals were acutely water deprived for 16-20 h and were presented with 20 % sucrose solution for 2 s, 3 times in the space of 10 min ("before"). Following that, they were repeatedly presented with drops of sucrose across a period of 10 min and were allowed to drink to satiation. 5 min after that the mice were carefully injected with LiCl as described above. 30 min after injection, mice were removed from the head-bar holder and returned to their cages with free access to water for 1h. After that, they were water deprived for 16-20 h, when they were head-fixed again and presented with 20 % sucrose solution for 2 s, 3 times in the span of 10 min ("after").

Optogenetic stimulation

Mice were tethered to optic patch cords and optogeneticaly stimulated with 473 nm light produced by a solid state laser (CNI Laser, China). The stimulation protocol was identical to all other stimuli, with the light being delivered for 2 s three times per experiment. The exact stimulation parameters were the following: aIC – bilateral 20 Hz stimulation, 10 ms pulse duration, 15 mW; pIC – bilateral 20 Hz stimulation, 10 ms pulse duration, 15 mW; VP: bilateral 40 Hz stimulation, 10 ms pulse duration, 15 mW; aIC→BLA, bilateral 20 Hz stimulation, 20 ms pulse duration, 10mW concurrent to 1mM quinine delivery. eYFP control mice were stimulated using the same parameters as mice expressing ChR2.

Freezing and Escape Detection

Freezing

We detected freezing episodes using a method we previously described (*22*), which establishes freezing in head-fixed animals as a combination of immobility, significant reduction in orofacial movements and a significant increase in pupil size lasting at least 2 s. We scored freezing when

either of two criteria was true: *either* an animal was immobile for at least 2 s with the z-scored pupil area was at least 1 sd higher than z-scored orofacial movement *or* a period of ≥ 5 seconds of immobility and complete lack of orofacial movements.

Pupil size measurements

We analyzed the pupil size similar to previous studies (*22*, *32*). In brief, for every frame we cropped the eye area, thresholded it to create a binary image and used the matlab function 'imfindcircles.m' to determine the pupil radius.

Orofacial movement analysis

Orofacial movements were analyzed as previously described (*33*).

Escape

Escape episodes were identified as periods of very rapid movement in a fearful context lasting at least 2 s as revealed by visual inspection.

Visualizations of typical facial expressions

Line drawings (Fig. 1B, right)

To illustrate the facial expression differences, an illustrator created line drawings of the facial outlines seen in the representative single video frames (Fig. 1B, left) selected from each emotion event.

Pixel difference heatmap overlays (Fig. 1B, right)

To visualize the areas of the face that are most changing in comparison the neutral facial expression, pixel difference heatmap overlays were created for each of the expressions in the following way: each of the example frames in Fig. 1B was pixel by pixel compared to the neutral expression frame by subtracting grayscale pixel values across the whole image. The results of this subtraction were then smoothed using a Gaussian filter with a sigma of 50 pixels, mapped to a color map, made partially transparent and overlaid over each of the original frames. Areas with almost no change were made transparent using a background removal tool for better visibility. The Gaussian filter was only applied for visualization purposes and not for data analysis.

Facial expression analyses

Motivation to employ the HOG feature approach to extract facial features of emotion

Comparing videos of behavioral features across animals is challenging because of transformations including translation, rotation, scale or changes in lighting between individuals. HOG features are designed to be largely invariant to these transformations. If the head position or illumination are slightly different between two animals, HOG will detect the pixel changes still in the same spatial grid and thus not notice these as different. Thus, the coarse binning and emphasis on orientation that HOG features provide, bear the advantage of greater invariance to changes in positioning, scale and lighting commonly occurring between different experiments. This invariance is crucial when comparing facial features across animals. Another advantage of the HOG feature extraction is the biologically inspired emphasis on edge detection. Indeed, while PCA was one of the first approaches to face recognition in humans (*34*), HOG features have been found to be superior to Eigen feature based face recognition approaches (*35*). Indeed, HOG and HOF (Histogram of optical flow) have been successfully employed in other studies of dynamic behavioral classification, especially when behavior had to be compared across individuals (*36*, *37*).

Histogram of oriented gradients descriptor creation

Histogram of oriented gradients (HOG) descriptors for each video frame were created using the following parameters: 8 histogram orientation bins, using square cells with a height of 32 pixels and 1 cell per block, with images normalized using power law compression before processing.

Similarity matrices

Face recordings of all experiments were processed using custom Python scripts. Each single frame was converted into a histogram of oriented gradients (HOG) vector. For all stimuli except LiCl injection, all frames during 4 s before the stimulus onset and 2 s during stimulus presentation, for 3 stimulus presentations, were pairwise compared (in total 540 frames). For the neutral condition, the procedure was the same, however, no actual stimulus was presented. For the LiCl injection, data was taken from a single experiment, where 3 sets of 4 s of baseline frames were selected in the first 2 minutes of experiment, after the mouse stopped exhibiting fear behaviors caused by the injection, but before malaise behavior would appear. The three 2 s long sets of stimulus frames were selected from frames 20 min after the start of experiment. A pairwise comparison of all selected frames per experiment was then performed by calculating Pearson's correlation coefficient for each possible pair and plotted in a hierarchically clustered

pairwise correlation matrix. The formed clusters were finally post-hoc compared to the frame temporal origins (before and during stimulus).

Prototypical face creation

All prototypical faces were created from a dedicated mouse whose data was not used in any other analysis. The generalizability of prototypes was tested independently and is exemplified in fig. S3A. First, a neutral prototypical facial expression was created by averaging HOGs of frames during a baseline period (250 frames) where no stimuli were presented and mouse was well habituated to the experimental setup. The validity of this baseline duration to best detect the deviations upon emotion events was independently tested and is shown in fig. S5B. The neutral prototypical face HOG was then compared to HOGs of frames during a single stimulus presentation for each of the identified states during clustering (above) by calculating a Pearson's correlation coefficient for each. For each of the states, 10 frames most dissimilar to the neutral prototypical face (the ones with the lowest correlation coefficient) were selected and averaged, resulting in a single HOG for each respective emotion. Prototypical faces were specifically build based on data associated with the following stimuli: disgust – 10mM quinine solution; pleasure – 20 % sucrose solution; malaise - 0.15 M LiCl i.p. injection; pain – 200 µA tail shock; passive fear - single detected freezing episode in a fearful context; active fear – single detected escape episode in fearful context. We independently confirmed that building the prototypes on medium stimulus intensities would still reveal scalable facial expressions. We found, however, that building the prototype on the strongest emotion event yielded the best prototype. The scalability was lost when prototypes were built on too low stimulus intensities (shown for pain in fig. S5C).

Mouse face registration and cropping

All data acquired using facial videography was registered to a single frame of a wild-type male mouse head-fixed to the setup exhibiting a neutral facial expression ("template frame"). This was achieved using custom written Python code employing a phase correlation approach, which enables estimation of relative offset of two similar images. For each recording, a single frame at the start of experiment was checked for optimal registration parameters, which were then applied across the whole recording. The image was first roughly aligned by being moved in relation to the template frame in the XY axis to the position of lowest offset, as indicated by phase correlation analysis. Following that, the image was angle aligned by being rotated for a single

degree at a time 45 degrees upwards and 45 degrees downwards, with the angle of lowest offset to the template frame being selected and applied. After correcting the rotation, the image was once again aligned in the XY axis. Finally, the image was scale matched to the template by rescaling it between 0.01 and 2 times in 0.01 steps and identifying the scale of lowest error based on phase correlation results, which was applied to the image as the final step. After the registration procedure was finished, the image was cropped using the same set of coordinates manually created to crop the template frame. The cropping coordinates were carefully selected to contain as little of non-face areas as possible, while not cutting off any of the face at a baseline facial expression, but also during any of the facial behaviors like licking. Attention was paid to also contain a section of empty space directly in front of the face in the template frame, since whiskers will move into that area during expressions such as pain and escape.

Similarity to prototypical face

To measure similarity to various prototypical faces, each acquired frame from any of the experiments was registered, cropped and converted into a HOG descriptor vector, as described above. Following that, each frame ("target frame") can be compared to a chosen prototypical face for similarity by calculating Pearson's r between the target frame HOG vector and the prototypical face HOG vector. If this is done across a single continuous experiment, the similarity comparison will result in a single similarity value per each time point, which can be plotted in a sequence, revealing a temporally evolving intensity graded description of experience.

Facial expression onsets and duration

We detected facial expression onsets (as in Fig. 3B, top) when the mean prototype similarity in a 1s bin was at least 2sd above baseline. The durations (as in Fig. 3B, bottom) were calculated from the number of consecutive 1s bin which were at least 2sd above baseline prototype similarity.

Classifiers

To confirm quantitative distinctiveness between facial expressions evoked by different stimuli or behaviors and create a tool that is able to separate any given set of frames into different discrete emotions, we created and trained a random forest classifier. The training dataset consisted of data collected from 3 animals, with 3 stimulus presentations for each emotion per each animal. We selected all 30 frames from the 2nd second of each stimulus presentation and appropriately

manually labeled them based on experimental origin. All frames were registered, cropped and converted into HOGs. Prior to classifier training, all HOG features corresponding to the area that could contain the spout (in all conditions whether spout was present or not), corresponding to the bottom right corner, size 4x9 HOG cells, were set to 0 to prevent any influence of the spout presence on prediction. To test the performance of the classifier, the training dataset was split into a smaller training dataset containing a randomly selected sample of 15% of all training data and tested on the remaining 85%. This was repeated 1000x, with the performance evaluated at each repetition. To establish a baseline performance to compare to, the classifier was trained and repeatedly tested in an exactly same manner, however, prior to training, all training dataset labels were randomly shuffled, while the performance was evaluated on the correctly labelled data.

Visualization of classifier feature importance (fig. S4)

To visualize importance of different sections of the face for decision 7 binary random forest classifiers were trained, one for each emotion state described in this manuscript, with all frames manually labeled as "1" (belonging to the emotion detected by the classifier) or "0" (not belonging to the specific emotion detected by the classifier). The data used for training was same as for the multiclass classifier described above, with the exception that no splitting into test and training datasets was performed. Since each HOG cell contains multiple orientation bins which cannot be easily visualized, the overall importance of each section of the frame was calculated as the mean feature importance of the 8 underlying orientation bins, for each classifier.

2-dimensional embedding of facial expressions

All video frames during the 2nd second of each stimulus presentation (30 frames) were collected for three stimulus repetitions for each respective stimulus/state. These frames were registered, cropped and converted into HOG vectors (5040 dimensions) and then dimensionality reduced using principal component analysis (100 dimensions). Following that, t-SNE (2 dimensions) was ran on the data of each respective mouse. The 2 t-SNE dimensions describing each data point were used to create a scatter plot, with each point representing a single frame. These points were finally post-hoc labeled based on the type of stimulus presented during their respective origins.

Optogenetic facial videography pipeline

To analyze the data collected in the optogenetic stimulation experiments, all frames at times of interest were first registered to the template frame, cropped and converted into HOG descriptors,

as described before (three 2s optogenetic stimulations per condition per animal). Frames belonging to a set of 3 stimulations from a single animal were then pairwise similarity compared by calculating Pearson's r for each pair and hierarchically clustered to reveal distinct groups of facial expressions corresponding to the peri-stimulus epochs. Following that, frames from the peri-stimulus epochs were processed using a random forest classifier trained on wild-type mice as described in the *classifier* section above. This resulted in a distribution of discrete emotion labels which guided selection of an appropriate prototypical face (based on the emotion most represented in the classifier detections). This prototypical face was then used as described above in the *Similarity to prototypical face section* to produce a graded readout of experience of the detected emotion.

Awake head-fixed two-photon imaging

Image acquisition

Two-photon imaging was carried out using a rotating resonant-scanning two-photon microscope (B-scope, Thorlabs) set to an angle perpendicular to the insular cortex surface (75 – 85° rotation to access the left hemisphere) with a 16x water immersion objective (Nikon N16XLWD-PF, N.A. = 0.8). This provided an 830 x 830 μm field of view that was scanned at 14.8 Hz with a resolution of 512 x 512 pixels. All imaged fields of view were imaged at a depth of 150-250 μm below the brain surface, using a Mai Tai DeepSee laser (Newport Corp.) set to 940 nm and a power of 12-30 mW at the front aperture of the objective.

Two-photon data pre-processing

Two-photon acquired neural data was processed using the two photon analysis toolbox Suite2p: https://github.com/MouseLand/suite2p (*38*), which was used to perform motion correction, neuron detection, cell-segmentation and fluorescence measurement over time for each cell. For each field of view, the cell segmentation was manually reviewed and corrected when necessary.

Neural data analyses

To quantify the degree of relatedness of each neuron's activity to either the facial expression or stimulus, we employed a previously described (*39, 40*) convolution approach to create predicted fluorescence traces for each (stimulus, facial expression) by convolving them with a GCaMP6s kernel. More specifically, we represented the stimulus as a square wave set to 1 when the stimulus was being presented (3 times 2s) and 0 everywhere else with a sampling rate of 30 Hz

and we used a relevant prototypical face similarity trace to represent the concurrent facial expression. Both of these were then convolved with a GCaMP6s kernel to produce a convolved stimulus trace and a convolved facial expression trace, which we compared to fluorescence of single neurons. Extracted fluorescence traces for each neuron were upsampled to facial videography sampling rate (30Hz), to enable comparison to both of the convolved traces, which we performed by calculating Pearson's r. We correlated each neuron to the relevant convolved stimulus traces and convolved facial expression trace. To determine which neurons were significantly correlated to either the face or the stimulus, we followed the approach described in (*40*). Specifically, we determined the thresholds for a significant correlation in an unbiased manner by calculating a null distribution for each imaging experiment by splitting all face/stimulus traces into 11 equally sized sections, randomly shuffled their temporal order, convolved the resulting traces and correlated them to fluorescence of all concurrently recorded neurons. This was repeated 1000 times for each dataset and the 99^{th} percentile of the resulting null distribution was chosen as the significant correlation threshold.

Human Raters Experiment

To evaluate whether untrained human observers would be able to detect emotional expression in mice, volunteers at a science outreach event answered a computer based questionnaire. Sixty-three human volunteers were shown single image examples of mice exhibiting neutral, passive fear, pleasurable, disgusted or painful facial expressions and asked two questions. 1) "Is this expression good or bad?" (Options to select good or bad) and 2) "What is the underlying experience?" (Options to select neutral, pleasure, disgust, fear and pain). We did not control for participant's age, sex or previous experience in working with mice.

Statistical Analysis

Analyses were performed using either Graphpad Prism (GraphPad Software, Inc., La Jolla, CA, USA, Version 8) or Python. Group comparisons were made using one-way ANOVA followed by Dunnett's post hoc tests comparing all groups to a baseline group in case main effect of ANOVA was statistically significant ($p < 0.05$). Two-group single variable comparisons were performed using a two-tailed Mann-Whitney U test. All correlation analyses were performed by calculating Pearson's correlation coefficient. To compare groups to a predetermined value, one sample two-sided Wilcoxon test was used. Detailed information about the type and results of all statistical

procedures can be found in Table S1. All animal numbers are reported in Figures and their legends. No statistical methods were used to predetermine sample size. Since we did not assume our data to be normally distributed we used nonparametric statistics except for the group comparisons in Fig. 2.

Supplementary Figures

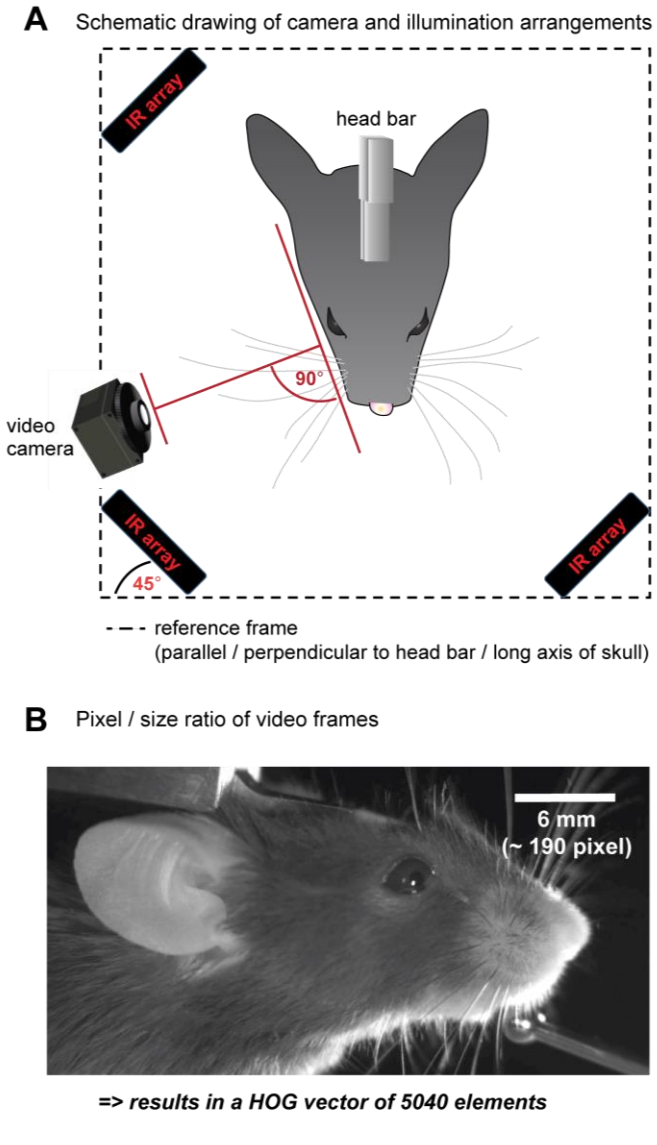

Fig. S1. Facial videography setup

(**A**) Illustration of camera and illumination arrangement with respect to the head of the mouse and the head bar. Three infrared arrays were used and mounted to a frame constructed around the head-fixation set-up. The frame was aligned to the head-bar and long-axis of the mouse skull as illustrated and infrared arrays were positioned at 45° angles to this frame. The camera was positioned at 90° to a virtual line along the mouse's lateral face surface. Camera positioning by hand was enough to ensure optimal video acquisition. We estimate that deviations of up to 15° from the ideal angle may still be tolerated as long as all facial features are in focus (ears, nose, eyes). The distances of camera and illumination to the head depended on the camera lenses used. Therefore, we illustrated in (**B**) the video frame resolution (cropped image that was used to create the HOG) with reference to the head size. We used a field of view of 1144 x 586 pixels, with a pixel resolution of approximately 30 pixels / mm. The mouse face registration and cropping procedure described in the methods section was employed to realign mouse faces and make them comparable, whenever camera angle and or distance varied between experiments.

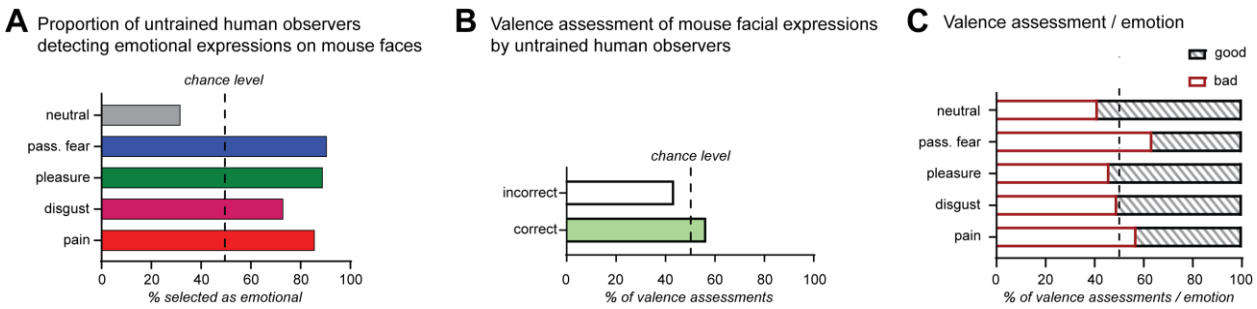

Fig. S2. Untrained human observers readily detect emotional facial expressions in mice.

Sixty-three human volunteers were asked in the context of a science outreach event to rate mouse facial expressions without further instructions. They were given two questions: 1) 'Is this expression good or bad?' and 2) 'What is the underlying experience?' (multiple choice format). (**A**) Untrained human observers reliably detected emotional expressions above chance and correctly rated neutral expressions as non-emotional. (**B**) The same observers failed to assign the correct valence (good or bad) to the emotional expressions. (**C**) However, a trend towards correctly classifying pleasure as good, but passive fear (freezing) and pain as bad was observed. Interestingly, also neutral expressions were more frequently rated as 'good'.

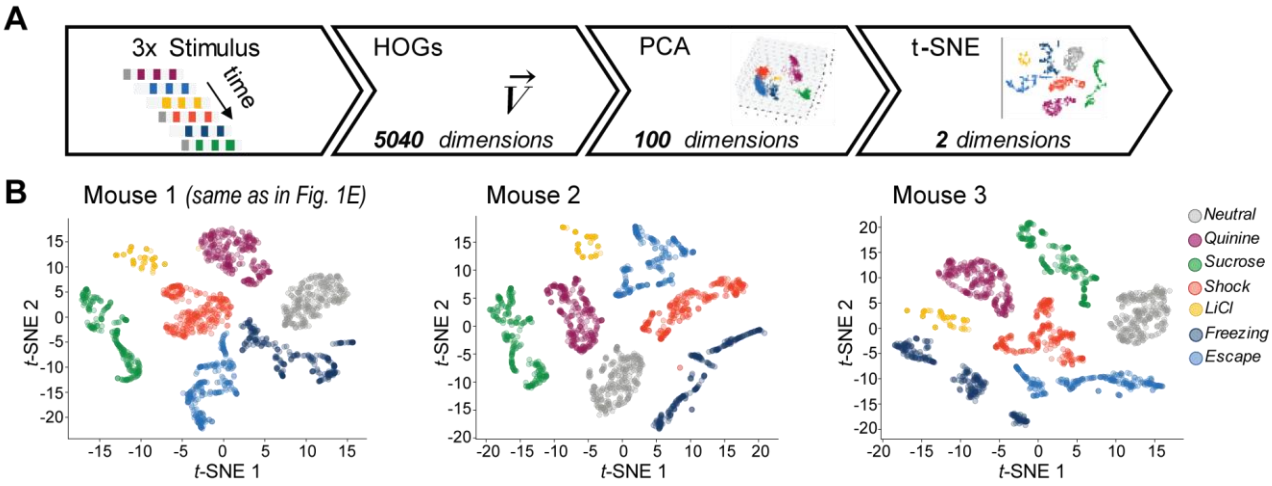

Fig. S3. t-SNE visualization in three individual mice.

(**A**) Analysis pipeline for t-SNE visualizations (**B**) t-SNE visualizations in each individual demonstrates clean separation into event-specific clusters.

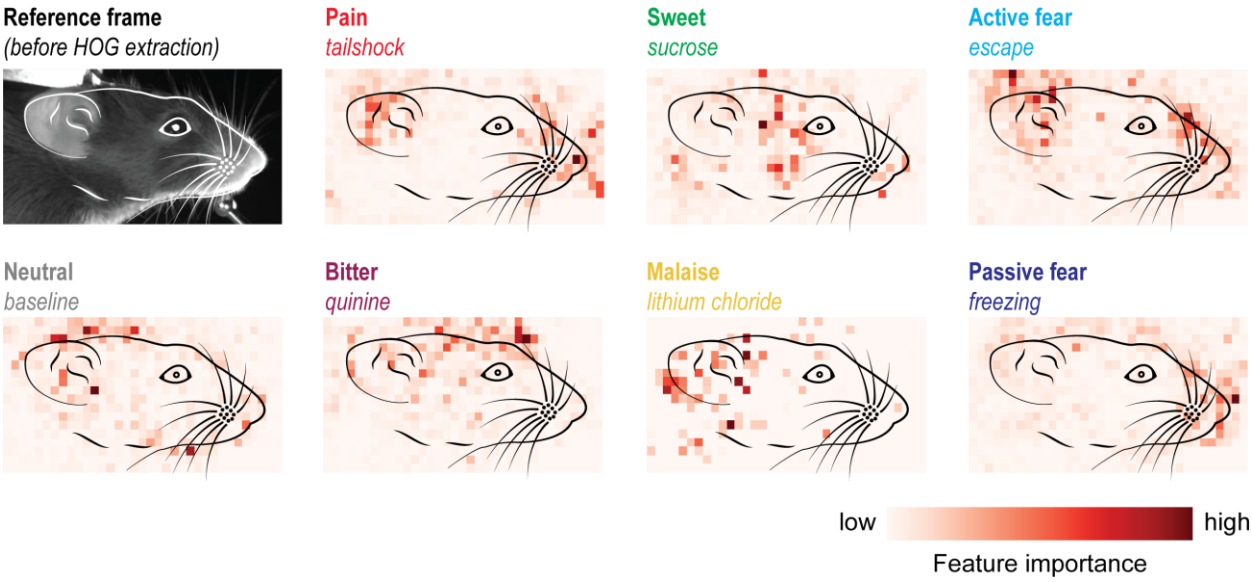

Fig. S4. Illustration of feature importance used by the random forest classifier to distinguish facial expressions of different emotion categories

The feature importance of HOG vector variables that were most decisive for the random forest classifier to distinguish different facial expressions were determined and the corresponding areas were color coded in an illustration. The color code depicts the level of feature importance to take a decision. A line drawing derived from the neutral expression is overlaid on all events to facilitate orientation.

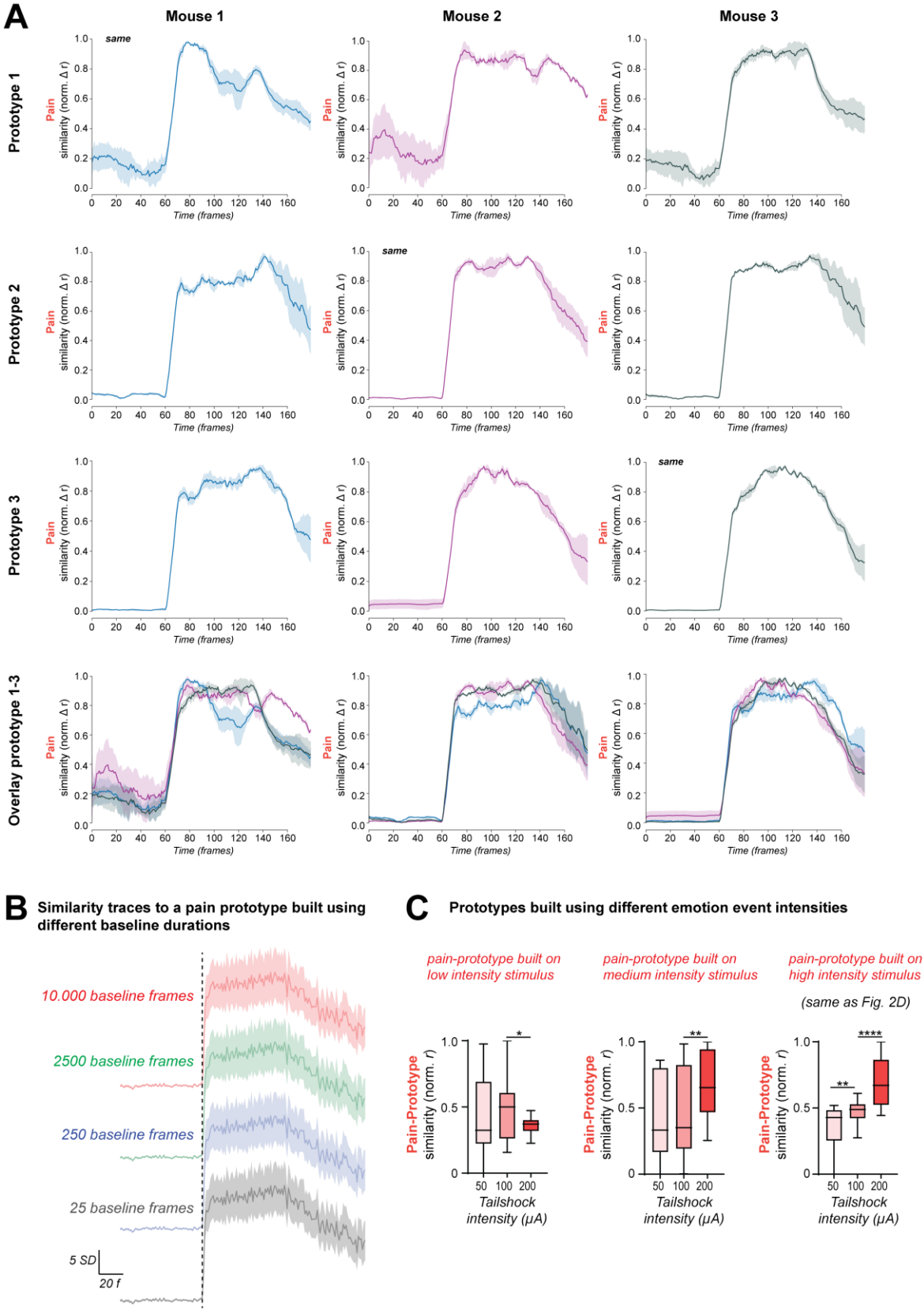
A
Mouse 1
Mouse 2
Mouse 3
Prototype 1
Prototype 2
Prototype 3
Overlay prototype 1-3
same
Pain similarity (norm. Δ r)
Time (frames)
B
Similarity traces to a pain prototype built using different baseline durations
10.000 baseline frames
2500 baseline frames
250 baseline frames
25 baseline frames
5 SD
20 f
C
Prototypes built using different emotion event intensities
pain-prototype built on low intensity stimulus
pain-prototype built on medium intensity stimulus
pain-prototype built on high intensity stimulus
(same as Fig. 2D)
Pain-Prototype similarity (norm. r)
Tailshock intensity (μA)

Fig. S5. Universality of emotion-prototypes.

(**A**) Prototypes can be built on any mouse and reveal stereotyped facial expressions in any other mouse. Here, as an example, we built one pain prototype on three individual mice and tested the validity of the prototype on each of them. All prototypes clearly reveal painful expressions in each of the mice. Notably, the prototype built and tested within the same mouse (marked as 'same') does not perform any better than a prototype built on a different mouse. Stimulus onset was at 60 frames = 2 s.

(**B**) Prototypes are built from frames the most different from a baseline ('neutral prototype'). Neutral prototypes are efficient in characterizing the emotion feature frames whether they are built from very few frames (25) or very many (2500, or 10.000). We here chose to build the neutral condition on 250 baseline frames.

(**C**) Prototypes can be built from differently strong emotion events. Comparing the scalability of emotions detected by similarities to prototypes on low, medium or strong stimulus intensities revealed that the best results are achieved when the prototype is built on the strongest emotion event. While prototypes built on medium intensity events still reveal scalability to some extent, this feature is lost when the prototype is built on the lowest stimulus intensity.

Two-tailed Mann-Whitney test: low intensity prototype (left), 50 vs. 100 µA: U = 288, P = 0.1902 and 100 vs 200 µA: U = 223, *P = 0.0137; medium intensity prototype (middle), 50 vs. 100 µA: U = 335, P = 0.6186 and 100 vs 200 µA: U = 188, **P = 0.0019; highest intensity prototype (right), 50 vs. 100 µA: U = 189, **P = 0.002 and 100 vs 200 µA: U = 127, ****P < 0.0001.

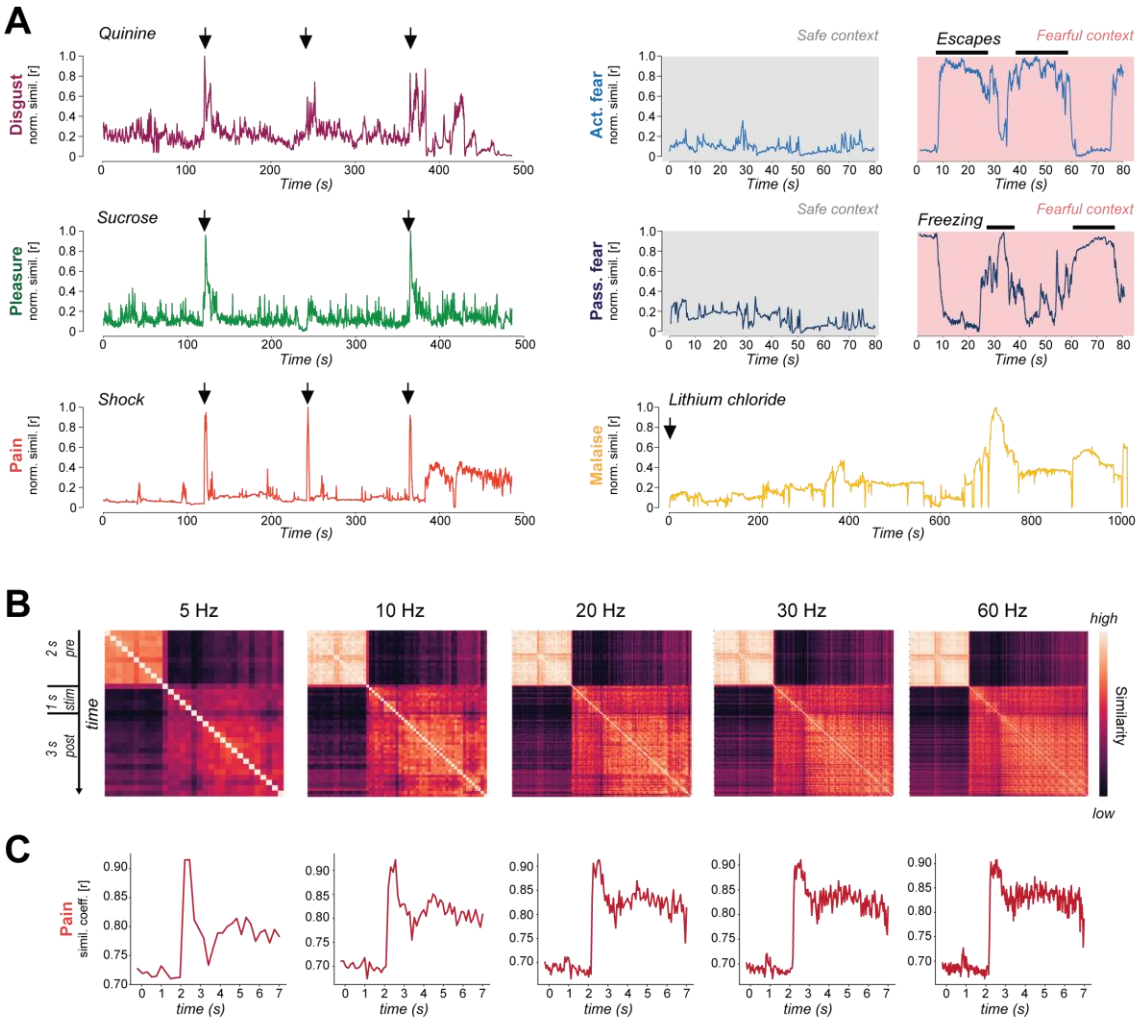

Fig. S6. Temporally resolved descriptions of facial expressions in mice.

(**A**) Exemplary similarity traces from individual animals to the prototypical expressions. Note that the face comparisons reveal diverse temporal dynamics of facial expressions in reaction to distinct stimuli / behavior onsets. All traces are from independent animals, except active and passive fear, which are the same expression compared to active and passive fear prototypes in a temporally aligned manner and while exposed to safe or fearful environments. Note the alternating pattern of freezing and escapes, which is reliably detected by facial tracking. Arrows denote stimulus onset. Horizontal black bars represent behavioral expressions.

(**B**) Comparison of different sampling frequencies (5-60 Hz) from one mouse experiencing a tailshock. The shock is administered for 1 second after 2 seconds. All frames were transformed into HOG vectors and pairwise similarity matrices were plotted. The HOG are plotted in temporal sequence of acquisition. Note that at all imaging frequencies the frames before the tailshock exhibit high similarity and are clearly distinct from the frames after tailshock.

(**C**) Similarity traces to the pain prototype built on all frames included within 400 ms during the tailshock at the different sampling rates. The shock is administered for 1 second after 2 seconds. Note that the similarity to the prototype is clearly detectable at all sampling frequencies. Higher sampling rates of 20-30 Hz reveal a more detailed description of the facial dynamics than a sampling rate of 5 Hz, however acquisition at 60 Hz does not qualitatively improve the facial description over 30 Hz.

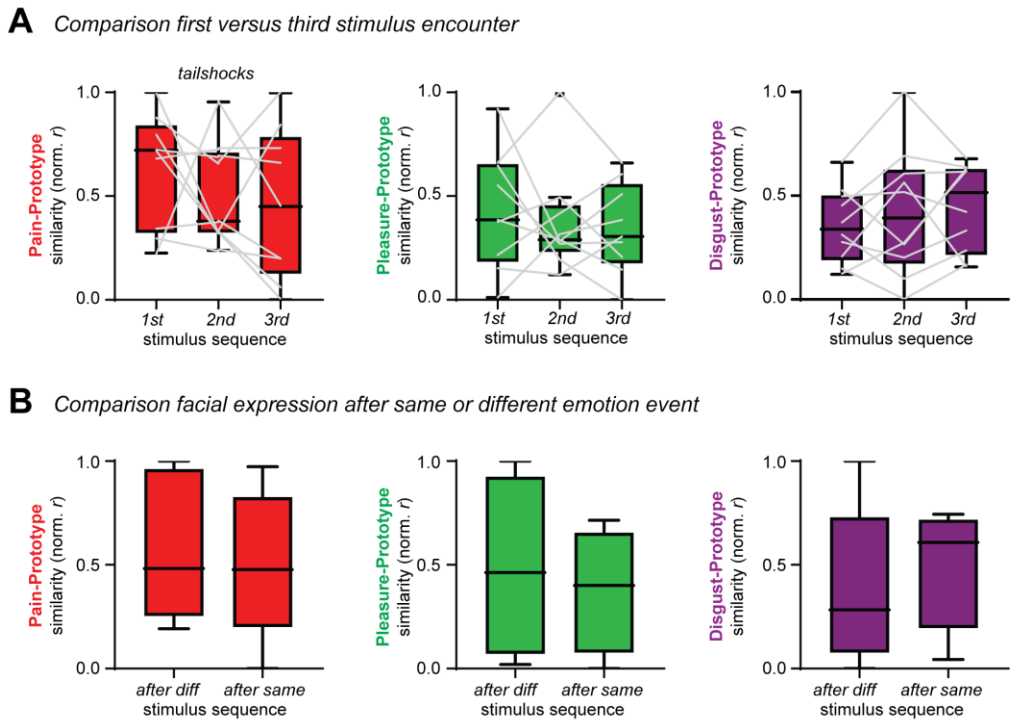

Fig. S7. Influence of stimulation sequence on emotional facial expressions (at 120 second ISI).

(**A**) Comparison of emotional facial expressions exhibited upon the first, second or third encounter of a given emotion event. The first encounter with a painful (tailshock), pleasurable (sucrose) or disgusting (quinine) stimulus does not evoke different facial expressions when compared to the third encounter. Box-and-whisker plots are Tukey style. Overlaid on the box-and-whisker plot are the changes from 1st to 3rd encounter in individual mice. N= 3 mice, n = 9 trials. Two-tailed RM one-way ANOVA: Left, pain: P = 0.3946, F (1.834, 14.67) = 0.9711; middle, pleasure: P = 0.6290, F (1.582, 12.66) = 0.4047; right, disgust: P = 0.4140, F (1.728, 15.55) = 0.8965.
(**B**) Comparison of emotional facial expressions following the same or a different emotion event. The facial expressions following the same type of emotion event do not consistently differ from the ones which follow the same type of emotion event. Box-and-whisker plots are Tukey style. Two-tailed Mann-Whitney U test: Left, pain: P = 0.8413, U = 11; middle, pleasure: P = 0.7302, U = 8; right, disgust: P = 0.5476, U = 9.

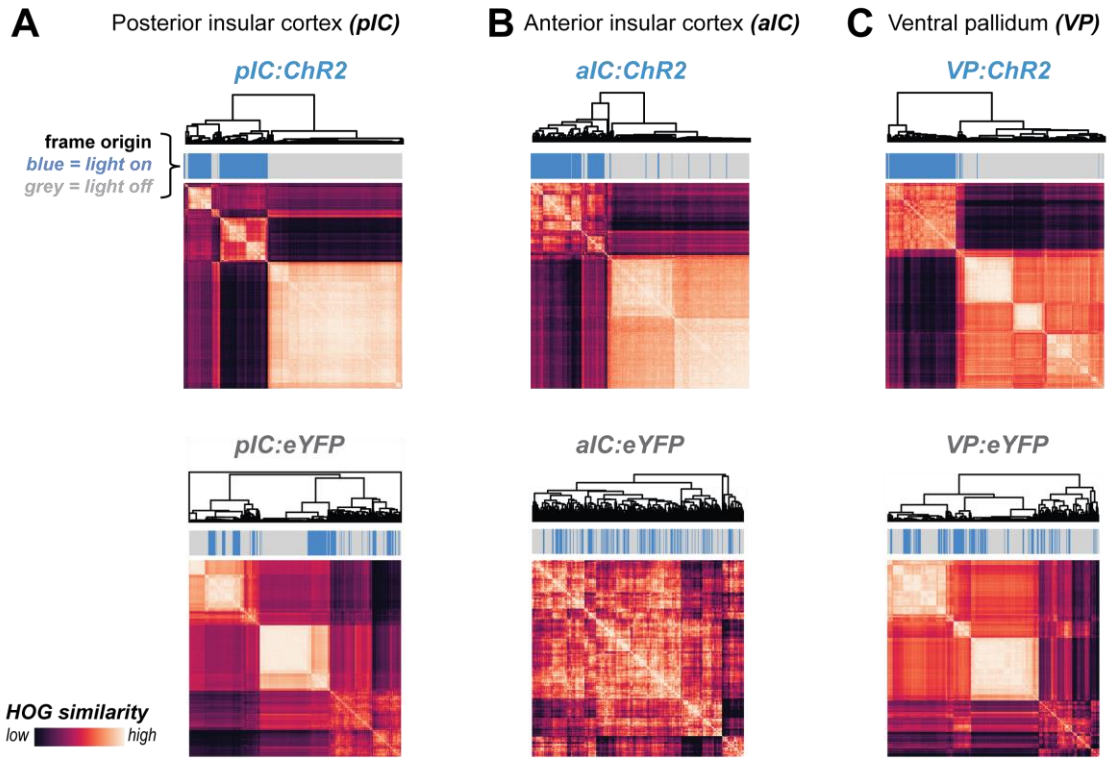

Fig. S8. Similarity matrices from individual animals exposed to optogenetic circuit manipulations.

(**A-C**) Top row: examples pairwise correlations of all frames before and during blue light stimulation for animals expressing channelrhodopsin. Bottom row: examples of pairwise correlations of all frames before and during blue light stimulation for animals expressing eYFP as control protein. Each mouse was stimulated three times for 2 second. Matrices are clustered in an unsupervised manner by similarity. Above the matrices are post-hoc temporal assignments with frames before the light in grey and frames during light in blue. Above the frame annotation are dendrograms revealing the clusters. Note the strong clustering of HOG vectors corresponding to the light *on* frames (blue) in channelrhodopsin-expressing animals which is absent in eYFP-expressing mice. The same is also revealed in the dendrograms on the top.

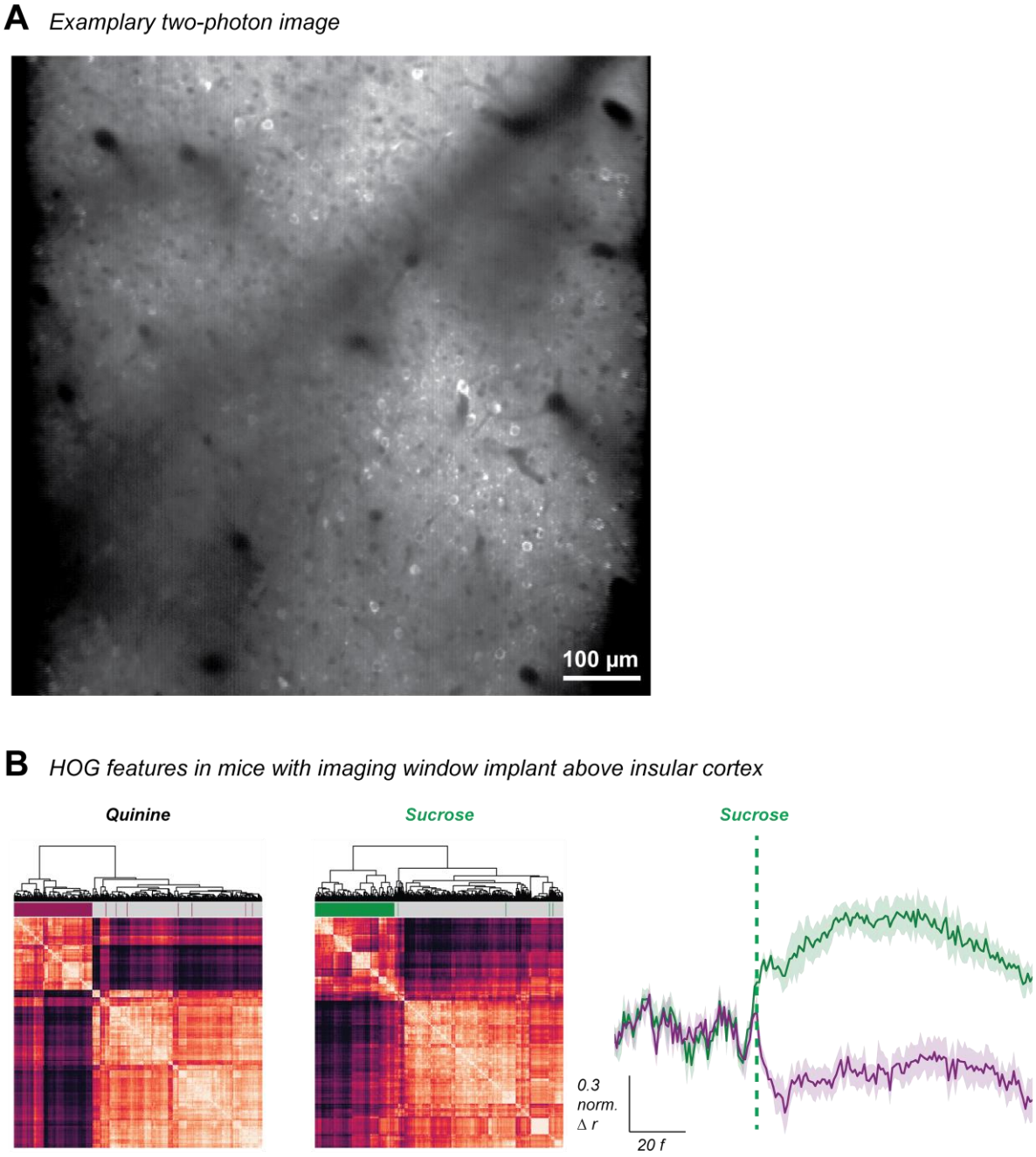

Fig. S9. Simultaneous two-photon imaging in the insular cortex and facial expression analyses.

(**A**) The same imaging field as shown in Fig. 4H. Image is a standard deviation projection of 7500 frames (i.e. ~500 s) imaged at 14.8 Hz. During this period, the animal was exposed three times for two seconds to a sucrose solution. The field of view is 830 x 830 µm large (resolution: 512 x 512 pixels).
(**B**) HOG-features before and during quinine- (left) or sucrose (middle) exposure cluster together in mice which had cranial-window implants above the left insular cortex, while facial features were analyzed from the right lateral facial surface. Right: Similarity to prototypical pleasure (green) or disgust (purple) face upon 3 exposures to 2-seconds of sucrose. HOG-extracted facial features are thus not affected by the implantation of a cranial window on the opposite side of the head. Shaded areas are s.e.m..

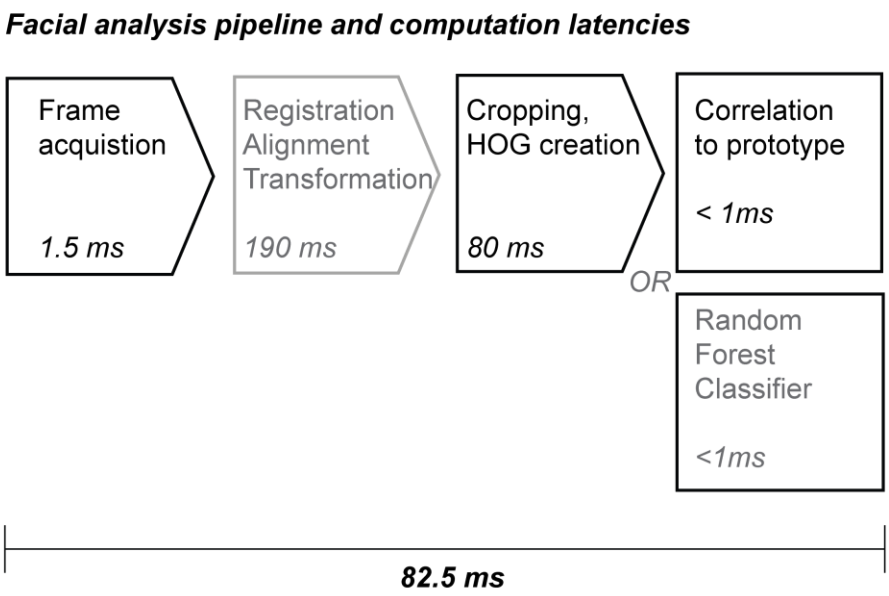

Fig. S10. Timeline of computation latencies.
Illustration of steps and latencies involved to acquire, process and compare/classify a live recorded video frame to a facial expression category. The registration, alignment and transformation step is only required when images were transformed between imaging sessions. When prototypes are build (or the classifier is trained) on animals from the same cohort and camera position, this step can be omitted. The total computation pipeline (total ~82.5 ms) can be run at 10 Hz and thus may allow for closed-loop configurations.

Table S1. Detailed statistics

Fig. 1F	Random forest classifier	neutral vs. shuffled neutral	Mann-Whitney test	two-tailed	U = 0	****P<0.0001
		disgust vs. shuffled disgust	Mann-Whitney test	two-tailed	U = 0	****P<0.0001
		pleasure vs. shuffled pleasure	Mann-Whitney test	two-tailed	U = 0	****P<0.0001
		malaise vs. shuffled malaise	Mann-Whitney test	two-tailed	U = 0	****P<0.0001
		pain vs. shuffled malaise	Mann-Whitney test	two-tailed	U = 0	****P<0.0001
		passive fear vs. shuffled passive fear	Mann-Whitney test	two-tailed	U = 0	****P<0.0001
		active fear vs. shuffled active fear	Mann-Whitney test	two-tailed	U = 0	****P<0.0001

Fig. 2C	Disgust prototype	Ordinary one-way ANOVA F (6, 182) = 20.53 ****P<0.0001	Quinine vs. neutral	Dunnett's	****	<0.0001
			Sucrose vs. neutral	Dunnett's	n.s.	0.9996
			LiCl vs. neutral	Dunnett's	n.s.	>0.9999
			Tailshock vs. neutral	Dunnett's	n.s.	0.8527
			Freezing vs. neutral	Dunnett's	n.s.	>0.9999
			Escape vs. neutral	Dunnett's	n.s.	>0.9999
	Pleasure prototype	Ordinary one-way ANOVA F (6, 182) = 33.42 ****P<0.0001	Quinine vs. neutral	Dunnett's	n.s.	0.3197
			Sucrose vs. neutral	Dunnett's	****	<0.0001
			LiCl vs. neutral	Dunnett's	n.s.	>0.9999
			Tailshock vs. neutral	Dunnett's	n.s.	>0.9999
			Freezing vs. neutral	Dunnett's	n.s.	>0.9999
			Escape vs. neutral	Dunnett's	n.s.	>0.9999
	Pain prototype	Ordinary one-way ANOVA F (6, 182) = 20.09 ****P<0.0001	Quinine vs. neutral	Dunnett's	n.s.	0.8267
			Sucrose vs. neutral	Dunnett's	n.s.	>0.9999
			LiCl vs. neutral	Dunnett's	n.s.	>0.9999
			Tailshock vs. neutral	Dunnett's	****	<0.0001
			Freezing vs. neutral	Dunnett's	n.s.	0.9954
			Escape vs. neutral	Dunnett's	n.s.	>0.9999
	Active fear prototype	Ordinary one-way ANOVA F (6, 182) = 22.81 ****P<0.0001	Quinine vs. neutral	Dunnett's	****	<0.0001
			Sucrose vs. neutral	Dunnett's	n.s.	0.9562
			LiCl vs. neutral	Dunnett's	n.s.	0.9562
			Tailshock vs. neutral	Dunnett's	****	<0.0001
			Freezing vs. neutral	Dunnett's	n.s.	>0.9999
			Escape vs. neutral	Dunnett's	****	<0.0001
	Pass. fear prototype	Ordinary one-way ANOVA F (6, 182) = 45.08 ****P<0.0001	Quinine vs. neutral	Dunnett's	n.s.	>0.9999
			Sucrose vs. neutral	Dunnett's	n.s.	>0.9999
			LiCl vs. neutral	Dunnett's	n.s.	>0.9999
			Tailshock vs. neutral	Dunnett's	n.s.	0.1420
			Freezing vs. neutral	Dunnett's	****	<0.0001
			Escape vs. neutral	Dunnett's	n.s.	>0.9999
	Malaise prototype	Ordinary one-way ANOVA F (6, 182) = 2428 ****P<0.0001	Quinine vs. neutral	Dunnett's	n.s.	>0.9999
			Sucrose vs. neutral	Dunnett's	n.s.	>0.9999
			LiCl vs. neutral	Dunnett's	****	<0.0001
			Tailshock vs. neutral	Dunnett's	n.s.	>0.9999
			Freezing vs. neutral	Dunnett's	n.s.	>0.9999
			Escape vs. neutral	Dunnett's	n.s.	>0.9999

Fig. 2D	tailshock strength	50 vs. 100 µA	Mann-Whitney test	two-tailed	U = 189	**P = 0.002
	tailshock strength	100 vs. 200 µA	Mann-Whitney test	two-tailed	U = 127	****P < 0.0001
	sucrose concentration	1% vs. 4 %	Mann-Whitney test	two-tailed	U = 192	**P = 0.0024
	sucrose concentration	4% vs. 20%	Mann-Whitney test	two-tailed	U = 236	*P = 0.0257
	quinine concentration	0.1mM vs. 1 mM	Mann-Whitney test	two-tailed	U = 294	*P=0.0207
	quinine concentration	1mM vs. 10mM	Mann-Whitney test	two-tailed	U = 291	*P=0.0181
Fig. 2E	salt – pleasure similarity	75 vs. 500mM	Mann-Whitney test	two-tailed	U = 43	**P=0.0031
	salt – disgust similarity	75 vs. 500mM	Mann-Whitney test	two-tailed	U = 47	**P=0.0055
Fig. 2F	sucrose – pleasure similarity	thirst vs. quenched	Mann-Whitney test	two-tailed	U = 33	***P=0.0006

	water – pleasure similarity	thirst vs. quenched	Mann-Whitney test	two-tailed	U = 10	****P<0.0001
Fig. 2G	pleasure similarity	sucrose before vs. after CTA learning	Mann-Whitney test	two-tailed	U = 0	****P<0.0001
	disgust similarity	sucrose before vs. after CTA learning	Mann-Whitney test	two-tailed	U = 12	****P<0.0001

Fig. 3F	Posterior insular cortex stimulation	One sample Wilcoxon test (sample: 0.1430)	Discrepancy: Neutral: -0.1430	Median and mean below sample	Median and mean below sample
			Discrepancy: Disgust: 0.8570	W = 66	p = 0.0039
			Discrepancy: Pleasure: -0.1430	Median and mean below sample	Median and mean below sample
			Discrepancy: Pain: -0.1430	Median and mean below sample	Median and mean below sample
			Discrepancy: Malaise: -0.1430	Median and mean below sample	Median and mean below sample
			Discrepancy: Act. Fear: -0.1430	Median and mean below sample	Median and mean below sample
			Discrepancy: Pass. Fear: -0.1430	Median and mean below sample	Median and mean below sample
Fig. 3F	Anterior insular cortex stimulation	One sample Wilcoxon test (sample: 0.1430)	Discrepancy: Neutral: -0.1430	Median and mean below sample	Median and mean below sample
			Discrepancy: Disgust: -0.1430	Median and mean below sample	Median and mean below sample
			Discrepancy: Pleasure: 0.8570	W = 171	p < 0.0001
			Discrepancy: Pain: -0.1430	Median and mean below sample	Median and mean below sample
			Discrepancy: Malaise: -0.1430	Median and mean below sample	Median and mean below sample
			Discrepancy: Act. Fear: -0.1430	Median and mean below sample	Median and mean below sample
			Discrepancy: Pass. Fear: -0.1430	Median and mean below sample	Median and mean below sample
Fig. 3F	Ventral pallidum stimulation	One sample Wilcoxon test (sample: 0.1430)	Discrepancy: Neutral: -0.1430	Median and mean below sample	Median and mean below sample
			Discrepancy: Disgust: -0.1430	Median and mean below sample	Median and mean below sample
			Discrepancy: Pleasure: 0.8370	W = 171	p < 0.0001
			Discrepancy: Pain: -0.1430	Median and mean below sample	Median and mean below sample
			Discrepancy: Malaise: -0.1430	Median and mean below sample	Median and mean below sample
			Discrepancy: Act. Fear: -0.1430	Median and mean below sample	Median and mean below sample
			Discrepancy: Pass. Fear: -0.1430	Median and mean below sample	Median and mean below sample

Fig. 3I	aIC→BLA stimulation	Pleasure no light versus with light	Mann-Whitney test	two-tailed	U = 28	P = 0.2973
		Disgust no light versus with light	Mann-Whitney test	two-tailed	U = 17	*P = 0.0400

Captions for Supplementary Movies

Movie S1

Facial videograph of a head-fixed mouse drinking sweet sucrose solution (left) or bitter quinine solution (right). Note the striking difference in facial expressions upon exposure to this appetitive or aversive experiences.

Movie S2

Simultaneous playback of the facial videograph of a facial expression of pain in reaction to a tailshock and a similarity plot (Pearson's r) to the prototypic pain expression built on a different mouse. Note the high specificity to the pain reaction.

Movie S3

Side-by-side comparison of the facial expression within the same mouse exposed to a sweet sucrose solution (left) or optogenetic stimulation of GABAergic neurons in the ventral pallidum (right). Note the striking similarity of the evoked facial expression.

References and Notes

1. C. Darwin, *The Expression of the Emotions in Man and Animals* (London, Murray, 1872).

2. A. Damasio, G. B. Carvalho, The nature of feelings: Evolutionary and neurobiological origins. *Nat. Rev. Neurosci.* **14**, 143–152 (2013). doi:10.1038/nrn3403 Medline

3. D. J. Anderson, R. Adolphs, A framework for studying emotions across species. *Cell* **157**, 187–200 (2014). doi:10.1016/j.cell.2014.03.003 Medline

4. Ralph Adolphs & David J. Anderson, *The Neuroscience of Emotion A New Synthesis* (Princeton Univ. Press, 2018).

5. R. Adolphs, How should neuroscience study emotions? by distinguishing emotion states, concepts, and experiences. *Soc. Cogn. Affect. Neurosci.* **12**, 24–31 (2017). doi:10.1093/scan/nsw153 Medline

6. J. A. Russell, A circumplex model of affect. *J. Pers. Soc. Psychol.* **39**, 1161–1178 (1980). doi:10.1037/h0077714

7. P. Ekman, An argument for basic emotions. *Cogn. Emotion* **6**, 169–200 (1992). doi:10.1080/02699939208411068

8. J. LeDoux, Rethinking the emotional brain. *Neuron* **73**, 653–676 (2012). doi:10.1016/j.neuron.2012.02.004 Medline

9. L. F. Barrett, A. B. Satpute, Historical pitfalls and new directions in the neuroscience of emotion. *Neurosci. Lett.* **693**, 9–18 (2019). doi:10.1016/j.neulet.2017.07.045 Medline

10. J. Panksepp, The basic emotional circuits of mammalian brains: Do animals have affective lives? *Neurosci. Biobehav. Rev.* **35**, 1791–1804 (2011). doi:10.1016/j.neubiorev.2011.08.003 Medline

11. P. Ekman, Facial expressions of emotion: An old controversy and new findings. *Philos. Trans. R. Soc. Lond. B Biol. Sci.* **335**, 63–69 (1992). doi:10.1098/rstb.1992.0008 Medline

12. L. A. Parr, B. M. Waller, J. Fugate, Emotional communication in primates: Implications for neurobiology. *Curr. Opin. Neurobiol.* **15**, 716–720 (2005). doi:10.1016/j.conb.2005.10.017 Medline

13. D. J. Langford, A. L. Bailey, M. L. Chanda, S. E. Clarke, T. E. Drummond, S. Echols, S. Glick, J. Ingrao, T. Klassen-Ross, M. L. Lacroix-Fralish, L. Matsumiya, R. E. Sorge, S. G. Sotocinal, J. M. Tabaka, D. Wong, A. M. J. M. van den Maagdenberg, M. D. Ferrari, K. D. Craig, J. S. Mogil, Coding of facial expressions of pain in the laboratory mouse. *Nat. Methods* **7**, 447–449 (2010). doi:10.1038/nmeth.1455 Medline

14. A. Faure, J. M. Richard, K. C. Berridge, Desire and dread from the nucleus accumbens: Cortical glutamate and subcortical GABA differentially generate motivation and hedonic impact in the rat. *PLOS ONE* **5**, e11223 (2010). doi:10.1371/journal.pone.0011223 Medline

15. K. Finlayson, J. F. Lampe, S. Hintze, H. Würbel, L. Melotti, Facial Indicators of Positive Emotions in Rats. *PLOS ONE* **11**, e0166446 (2016). doi:10.1371/journal.pone.0166446 Medline

16. J. Chikazoe, D. H. Lee, N. Kriegeskorte, A. K. Anderson, Population coding of affect across stimuli, modalities and individuals. *Nat. Neurosci.* **17**, 1114–1122 (2014). doi:10.1038/nn.3749 Medline

17. N. Gogolla, The insular cortex. *Curr. Biol.* **27**, R580–R586 (2017). doi:10.1016/j.cub.2017.05.010 Medline

18. P. Tovote, J. P. Fadok, A. Lüthi, Neuronal circuits for fear and anxiety. *Nat. Rev. Neurosci.* **16**, 317–331 (2015). doi:10.1038/nrn3945 Medline

19. N. Dalal, B. Triggs, in *2005 IEEE Computer Society Conference on Computer Vision and Pattern Recognition, CVPR 2005* (2005), vol. 1, pp. 886–893.

20. F. Caruana, A. Jezzini, B. Sbriscia-Fioretti, G. Rizzolatti, V. Gallese, Emotional and social behaviors elicited by electrical stimulation of the insula in the macaque monkey. *Curr. Biol.* **21**, 195–199 (2011). doi:10.1016/j.cub.2010.12.042 Medline

21. C. Fausto, The integration of emotional expression and experience: A pragmatist review of recent evidence from brain stimulation. *Emot. Rev.* **11**, 27–38 (2019). doi:10.1177/1754073917723461

22. D. A. Gehrlach, N. Dolensek, A. S. Klein, R. Roy Chowdhury, A. Matthys, M. Junghänel, T. N. Gaitanos, A. Podgornik, T. D. Black, N. Reddy Vaka, K.-K. Conzelmann, N. Gogolla, Aversive state processing in the posterior insular cortex. *Nat. Neurosci.* **22**, 1424–1437 (2019). doi:10.1038/s41593-019-0469-1 Medline

23. J. Yih, D. E. Beam, K. C. R. Fox, J. Parvizi, Intensity of affective experience is modulated by magnitude of intracranial electrical stimulation in human orbitofrontal, cingulate and insular cortices. *Soc. Cogn. Affect. Neurosci.* **14**, 339–351 (2019). doi:10.1093/scan/nsz015 Medline

24. Y. Peng, S. Gillis-Smith, H. Jin, D. Tränkner, N. J. P. Ryba, C. S. Zuker, Sweet and bitter taste in the brain of awake behaving animals. *Nature* **527**, 512–515 (2015). doi:10.1038/nature15763 Medline

25. L. Wang, S. Gillis-Smith, Y. Peng, J. Zhang, X. Chen, C. D. Salzman, N. J. P. Ryba, C. S. Zuker, The coding of valence and identity in the mammalian taste system. *Nature* **558**, 127–131 (2018). doi:10.1038/s41586-018-0165-4 Medline

26. L. Faget, V. Zell, E. Souter, A. McPherson, R. Ressler, N. Gutierrez-Reed, J. H. Yoo, D. Dulcis, T. S. Hnasko, Opponent control of behavioral reinforcement by inhibitory and excitatory projections from the ventral pallidum. *Nat. Commun.* **9**, 849 (2018). doi:10.1038/s41467-018-03125-y Medline

27. X. Chen, M. Gabitto, Y. Peng, N. J. P. Ryba, C. S. Zuker, A gustotopic map of taste qualities in the mammalian brain. *Science* **333**, 1262–1266 (2011). doi:10.1126/science.1204076 Medline

28. C. Montag, J. Panksepp, Primal emotional-affective expressive foundations of human facial expression. *Motiv. Emot.* **40**, 760–766 (2016). doi:10.1007/s11031-016-9570-x

29. J. M. Susskind, D. H. Lee, A. Cusi, R. Feiman, W. Grabski, A. K. Anderson, Expressing fear enhances sensory acquisition. *Nat. Neurosci.* **11**, 843–850 (2008). doi:10.1038/nn.2138 Medline

30. L. F. Barrett, R. Adolphs, S. Marsella, A. M. Martinez, S. D. Pollak, Emotional expressions reconsidered: Challenges to inferring emotion from human facial movements. *Psychol. Sci. Public Interest* **20**, 1–68 (2019). doi:10.1177/1529100619832930 Medline

31. N. Dolensek, N. Gogolla, GogollaLab/MouseFacialExpressionAnalysis, Version 1.0, Zenodo (2020). http://doi.org/10.5281/zenodo.3618395

32. J. B. Wekselblatt, E. D. Flister, D. M. Piscopo, C. M. Niell, Large-scale imaging of cortical dynamics during sensory perception and behavior. *J. Neurophysiol.* **115**, 2852–2866 (2016). doi:10.1152/jn.01056.2015 Medline

33. Y. Livneh, R. N. Ramesh, C. R. Burgess, K. M. Levandowski, J. C. Madara, H. Fenselau, G. J. Goldey, V. E. Diaz, N. Jikomes, J. M. Resch, B. B. Lowell, M. L. Andermann, Homeostatic circuits selectively gate food cue responses in insular cortex. *Nature* **546**, 611–616 (2017). doi:10.1038/nature22375 Medline

34. M. P. H. Gardner, A. Fontanini, Encoding and tracking of outcome-specific expectancy in the gustatory cortex of alert rats. *J. Neurosci.* **34**, 13000–13017 (2014). doi:10.1523/JNEUROSCI.1820-14.2014 Medline

35. M. Turk, A. Pentland, Eigenfaces for recognition. *J. Cogn. Neurosci.* **3**, 71–86 (1991). doi:10.1162/jocn.1991.3.1.71 Medline

36. H. S. Dadi, G. K. Mohan Pillutla, Improved face recognition rate using HOG features and SVM classifier. *IOSR J. Electron. Commun. Eng.* **11**, 34–44 (2016). doi:10.9790/2834-1104013444

37. B. A. Sauerbrei, J. Z. Guo, J. D. Cohen, M. Mischiati, W. Guo, M. Kabra, N. Verma, B. Mensh, K. Branson, A. W. Hantman, Cortical pattern generation during dexterous movement is input-driven. *Nature* **577**, 386–391 (2020). 10.1038/s41586-019-1869-9 Medline

38. I. S. Kwak, J.-Z. Guo, A. Hantman, D. Kriegman, K. Branson, Detecting the starting frame of actions in video . arXiv:1906.03340 [cs.CV] (2019).

39. M. Pachitariu *et al.*, Suite2p: beyond 10,000 neurons with standard two-photon microscopy. bioRxiv 061507 [Preprint]. 20 July 2017. https://doi.org/10.1101/061507.

40. A. Miri, K. Daie, R. D. Burdine, E. Aksay, D. W. Tank, Regression-based identification of behavior-encoding neurons during large-scale optical imaging of neural activity at cellular resolution. *J. Neurophysiol.* **105**, 964–980 (2011). doi:10.1152/jn.00702.2010 Medline

41. R. Portugues, C. E. Feierstein, F. Engert, M. B. Orger, Whole-brain activity maps reveal stereotyped, distributed networks for visuomotor behavior. *Neuron* **81**, 1328–1343 (2014). doi:10.1016/j.neuron.2014.01.019 Medline